

Dear Dr. Elvidge (Referee, Geoscientific Model Development),

thank you for your reviewer report from 3 August 2016. We have accounted for the comments and suggestions in the revised manuscript version. Please find our replies to the particular comments in the following.

Sincerely,

Konrad Deetz and Bernhard Vogel

Referee comments:

1) The VIIRS Night Fire (VNF) "flares only" dataset is not suitable for scientific applications. It is generated by stripping out VNF detections with either no temperature or temperatures under 1400K. This eliminates most biomass burning and ambiguous detections. The purpose of this is to provide a quick daily overview of global gas flaring activity. There are many times when a flare was detected in a single spectral band (usually M10 at 1.6 μm), in which case the Planck curve cannot be fit and a temperature cannot be calculated. These detections have been lost in the dataset used by the authors. In addition, some flares are known to fluctuate in temperature and dip below 1400 K. These low temperature flaring events are also lost in the "flares only" daily summaries. To produce a more thorough analysis, the authors should work from the original daily VNF files. At best the "flares-only" version of the data provides a 'quick-and-dirty' depiction of global gas flaring.

For our work in the project Dynamics-aerosol-chemistry-cloud interactions in West Africa (DACCIWA) we wanted to have a consideration of gas flaring in our regional atmospheric model which includes the up-to-date characteristics of southern West Africa (SWA). The DACCIWA measurement campaign took place in June/July 2016 and for this time we need the flaring information for our model. Emission estimates for 2012/2013/2014 are not meaningful in our case, because the emissions are not constant from year to year. Also your new estimation (http://ngdc.noaa.gov/eog/viirs/download_global_flare.html) shows a decrease in flaring for Nigeria. To use older data would lead to overestimations.

The SWA emission inventory for flaring was not available when we started our research. The presented method is therefore our first approach to tackle the problem with the missing flaring emissions in our atmospheric chemistry simulations. Instead of using just constant emissions factors for flaring, we now have very regional information available.

We are concentrating on the description of the air pollution in our modelling system COSMO-ART and try to include all relevant emission sources. We are not experts in extracting the flaring sources from the general combustion sources detected by VIIRS Nightfire. Therefore we have relied on the "flares only" product published at http://ngdc.noaa.gov/eog/viirs/download_viirs_flares_only.html. Even if the data basis for our study is not perfect regarding VNF, there is a strong progress compared to the state before. We have changed our manuscript according to this problem. We have remarked, that the use of the "flares only" product is just a first approach and that this data contains greater uncertainties compared to the original VNF product. Future users of this parameterization can change the VNF input. The general method of the parameterization will not be affected by that.

2) The authors do not account for variations in cloud cover. This can be done based on the VIIRS Cloud product suite.

I see your point but our study focus is located to the creation of an emission dataset based on a VNF climatology rather than taking the VNF data day by day. In section 3.3.1 we describe the problem of flares that are masked by clouds (and the overall question whether the flare below the cloud is active or not) in detail and assess the uncertainty by using remote sensing cloud data from MSG and Aqua/AIRS. By deriving a flaring climatology (over two month), we are able to identify all flares (even if there are sometimes covered by clouds). With this climatological approach we get the mean emission strength of every flare (more precisely for every flare box). Therefore it is not necessary to account for the variations in cloud cover. Even if we would know, that a certain flare is masked by clouds at a certain day we don't know whether this flare is currently active and how large the radiant heat is. When we use our flaring climatology in our regional atmospheric model, all available flares are active at once with their mean emission strength.

3) The text should reference the following paper: Methods for Global Survey of Natural Gas Flaring from Visible Infrared Imaging Radiometer Suite Data (<http://www.mdpi.com/1996-1073/9/1/14>).

We agree on that and have referenced the publication.

4) NOAA has global flaring data spanning 2012-2014 available at: http://ngdc.noaa.gov/eog/viirs/download_global_flare.html. There is a csv that contains locations and annual summaries of temperatures and radiant heat output of individual flares, normalized for cloud cover. The flared gas volume estimates are derived from an empirical calibration with CEDIGAZ reported flaring. It would be interesting to compare the NOAA results with those from the methods described in this paper.

From the xlsx file VIIRS_Global_flaring_d.7_slope_0.331_web.xlsx we have selected the 193 available Nigerian upstream flares and selected the flares which have a detection frequency greater than zero for 2014. We assume that "Avg. K" mean source temperature in K and "Ellipticity" means the radiant heat in MW. This data we have used as input for the parameterization presented in this study (with the same configuration). Finally we have integrated the volume stream of all Nigerian flare boxes from m-3 s-1 to m-2 y-1 and finally transformed it to bcm. The result is 8.55 bcm (271.0391 m-3 s-1). In the xlsx file the flared volume is estimated as 8.442995283 bcm for Nigeria in 2014. So if we use the same source temperature and radiant heat input as Elvidge et al. (2015) for Nigeria in 2014, we can reproduce the estimated flared volume with our method with a deviation below 1.3%.

Within our VNP data set for 2014 we estimate the flaring to 29.8 bcm. Regarding the uncertainty range of this estimation, the value is approx. by a factor of two higher than the other inventory. The uncertainty might result from the uncertainties in the estimation of the gauge pressure p_g and the fraction of the total reaction energy that is emitted as radiation f . In our flaring climatology we assume that all available flares are active at once with their mean emission strength, so this could lead to the higher values of the flared volume.

5) In the last sentence of the first paragraph, the text references the World Bank for a set of national flared gas volume estimates. The text should make it clear that these estimates were produced by NOAA using DMSP satellite data. There is a new set of estimates derived from VIIRS data at http://ngdc.noaa.gov/eog/viirs/download_global_flare.html.

We agree on that and have changed the manuscript accordingly. A remark to the availability of updated global flaring estimates for 2013 and 2014 at http://ngdc.noaa.gov/eog/viirs/download_global_flare.html are mentioned in the manuscript.

Dear Dr. Elvidge (Referee, Geoscientific Model Development),

thank you for your reviewer report from 5 August 2016. We have accounted for the comments and suggestions in the revised manuscript version. Please find our replies to the particular comments in the following.

Sincerely,

Konrad Deetz and Bernhard Vogel

Referee comments:

1.) Being fully familiar with the flares only version of the VIIR Nightfire product I can certify that this product is not suitable for use in a scientific study. If the authors had contacted my team at the start of their study we could have explained this to them and directed them to the full VNF data files, which are suitable for use in scientific studies.

2.) NOAA does provide cloud state for each VNF detection - from the VIIRS cloud product suite. There are four states: confidently cloudy, probably cloudy, probably clear, confidently clear. But what is not recorded in the VNF files are the number of clear observations where the flare was not detected. The NOAA annual gas flaring data takes this into account. I dispute the authors contention that "it is not necessary to account for the variations in cloud cover."

3.) My overall impression is that these authors are willing to use data that are known to be flawed and ignore the effects of cloud cover variations in order to get a paper published without doing any additional work. If this journal is willing to publish papers with flaws like this disclosed - heaven help them.

The authors are puzzled about the different tenor in the two reviews we have achieved from you. We regret that you have the impression we are not willing to invest additional work for this study. Under point 4 of our reply from 3 August 2016 we followed your idea to compare your dataset with our study. Maybe one of your team can give us information on how to use the full VNF data files correctly and how to separate the flaring sources from other combustion sources (e.g. forest fires). With this data set, under consideration of the cloud correction, we will repeat our study.

M. Zhizhin provided us with the full VNF data for the relevant SWA countries in the time period of interest. The study has been repeated based on the new data and including the VIIRS cloud product.

Dear Mikhail Zhizhin (Referee, Geoscientific Model Development),

thank you for your reviewer report from 14 October 2016. We have accounted for the comments and suggestions in the revised manuscript version. Please find our replies to the particular comments in the following.

We have uploaded a revised manuscript which also includes the revision regarding the comments and suggestions of the first reviewer.

Sincerely

Konrad Deetz and Bernhard Vogel

Referee comments:

In the paper a new method to model emissions from gas flaring is developed and validated on oil fields in Western Africa. The paper is a substantial contribution to the modeling science, and the approach is valid and motivating for further research. I have some comments on the presentation and details of the method which could be considered by the Authors before it is published.

0. I would recommend changing abbreviation VNP (VIIRS Nightfire Product) to commonly used VNF (simply VIIRS Nightfire) in the manuscript.

We agree on that and have changed the manuscript accordingly. For the general VIIRS Nightfire (including all combustion sources) we use the abbreviation “VNF” and for the extracted flaring information from VNF we use the abbreviation “VNF_{flare}”.

1. Formula (1) derives gas flow rate from flare radiative heat and temperature measured from satellite. It is a basis of the proposed model. However, it is taken from Appendix of regulating document by the German Environmental protection agency. This is technical, not scientific source. The derivation of the formula is not provided neither in the paper under review, nor in the cited document. The cited document has no source for the formula either. It is important to derive the formula (1) or to provide a scientific reference.

We agree on that. TA-Luft is a technical document and the equation is not well introduced there. Equation 1 of the manuscript originates from VDI 3782, 1985: Dispersion of Air Pollutants in the Atmosphere, Determination of Plume rise, Verein Deutscher Ingenieure, VDI-Richtlinien 3782 Part 3, Equation 24, https://www.vdi.de/richtlinie/vdi_3782_blatt_3-ausbreitung_von_luftverunreinigungen_in_der_atmosphaere_berechnung_der_abgasfahnenueberhoehung/ (accessed: October 17, 2016). We have changed the citation accordingly. Although VDI 3782 (1985) is also a technical document, the derivation of the equation becomes clear. The heat flow M in MW is given by equation 1

$$M = c_p F (T_S - T_A), \quad (1)$$

where F is the flow rate in $\text{m}^3 \text{s}^{-1}$, c_p the mean specific heat capacity of the emissions, T_S the source temperature and T_A the ambient temperature. VDI 3782 (1985) provides a value of the mean specific heat capacity of

$$c_p = 1.36 \cdot 10^{-3} \text{ MW s m}^{-3} \text{ K}^{-1}$$

which is derived for a pit coal firing but VDI 3782 (1985) denotes, that this can be used for other flue gases as well since potential deviations are negligible. (An explicit c_p value for gas flaring is not provided in the literature.) For the ambient temperature T_A we use 298.15K as a fixed value, representative for the tropical region. Within a sensitivity study regarding the influence of T_A on F we have used the mean heat flow and the mean source temperature of all flares in TP15 and varied the ambient temperature between 293K and 303K, as

a reasonable temperature range in the tropical regions. The resulting maximum difference in the heat flow is 0.0036 m³ s⁻¹. Therefore we assume the errors using a fixed climatological value for the ambient temperature are negligible, but of course the user has to adapt the ambient temperature to the region he wants to apply the inventory. We have emphasized this in the manuscript. By using equation 1, the value for c_p and for T_A , the flow rate F in MW is given by:

$$F = M / (1.36 \cdot 10^{-3} (T_S - 298.15)). \quad (2)$$

2. Flare temperature used in the formula (1) is taken from instantaneous satellite measurement (VNF). It has a large variance depending on atmospheric conditions etc. I would recommend using mean flare temperature averaged over all cloud-free detections.

We see your point. This leads to a further source of uncertainty, because we cannot decide whether the spatial source temperature variations really results from the sources or from the atmospheric conditions. We think that this problem does not affect the climatological approach (E_{clim} in the revised manuscript) because for every detected flare the source temperature already is averaged over the two-month period of TP14 or TP15 before we calculate the emissions. We assume that this is a compromise between robustness and keeping the spatial variability of the flaring. To allow for consistency we now also use these temporal averages of source temperature and radiant heat for the daily resolved inventories (E_{obs} and E_{com} in the revised manuscript). Therefore all three inventories have the same underlying emission field and the difference is just related to number of flares that are active at a certain day. For E_{clim} all flares are active at once, for E_{obs} only the actual observed flares are active and for E_{com} the actual observed flares + the cloud covered flares (taken as active) are considered (com=combination). Nevertheless we have also included a further inventory in Tab. 5 that uses instantaneous input data to derive E_{clim} (first calculating the emissions for every single observation and then averaging the emissions temporally). This is given as “ E_{clim} , instant. input” and should allow further insight in the sensitivity/uncertainty.

3. The number 283 used in the formula (1) I believe stands for ambient air temperature at night? Is it a proper climatological value for Wester Africa?

Yes, the 283 refers to the ambient temperature. We agree that this value is not appropriate for the tropics. We have changed this value in the manuscript to 25°C (298.15K, also described in Comment 1 of this document). Owing to the change of the ambient temperature we have repeated our analysis to be consistent with this new value. The change from $T_A = 283K$ to 298.15K lead to a slight increase in the emissions (e.g. for Fig. 9b the spatially integrated SWA emissions of TP14 increase from 651 to 658 t h⁻¹).

4. Comments 1-3 may result in a wider variance of the proposed model output, and the model sensitivity analysis should be presented.

Regarding the ambient temperature (Comment 3) we have presented the maximum uncertainty in the heat flow as 0.0036 m³ s⁻¹, which is also described in the manuscript. For the mean heat capacity of the emission c_p we do not have further information to assess the uncertainty. For considering the uncertainty in using temporal averages of source temperature and radiant heat instead of the instantaneous satellite observations, we have added a further emission inventory in Tab. 5 (“ E_{clim} , instant. input”, for TP14 and TP15).

5. The Authors have made a considerable effort to take into account cloud conditions which can mask flare observations from space. Why not to use only cloud-free observation days, and to count detected/not detected flare cases to derive mean radiative heat?

By using the postprocessed flaring data (VNF_{flare} in the revised manuscript which includes also a cloud mask) instead of the “Flaring only” product, it is straightforward to separate the flares into the categories (a) “cloud-covered”, (b) “cloud-free and inactive” and (c) “cloud-free and active”. By assuming that the cloud-covered flares are active with their mean emission strength, we can estimate the daily emissions via the sum of (a) and (c). To use only the cloud-free observation days would be problematic because SWA is a region with very extensive cloud cover (on average approx. 70% in the flaring area).

I would like to acknowledge that the Authors provide software sources and input data used in the study as the paper supplement. It is helpful for reproduction and reuse of their science and model.

List of relevant changes

1. Use flaring information from “VIIRS Nightfire Nighttime Detection and Characterization of Combustion Sources” instead of the quick-look data from “VIIRS Nightfire (Flares Only version). The study has been repeated with this data.
2. More detailed description and derivation of Equation 1.
3. Add missing references.
4. Based on the availability of the VIIRS cloud product, the strategy of assessing the uncertainty of flares masked by clouds has been changed. Three categories were defined: (1) cloud-free and active, (2) cloud-free and inactive, (3) cloud-covered and assumed to be active. This leads to different emission inventories. We have defined two inventories in addition to the climatology (E_{clim}): (a) E_{obs} which only consider the daily observations and (b) E_{com} which is a combination of E_{obs} and the emission from the cloud-covered flares.
5. Assessment of a further source of uncertainty regarding instantaneous VIIRS observations vs. averaged VIIRS observations. This assessment lead to a further emission inventory: $E_{\text{clim, inst}}$, instantaneous input.
6. Additionally, the sensitivity of the flow rate calculation in Eq. 1 towards the ambient temperature has been assessed.
7. Correction of the ambient temperature in Eq. 1 to consider tropical conditions. For consistency the study has been repeated.
8. Update of Tab. 5 based on the revised analysis.

Development of a new gas flaring emission data set for southern West Africa

Konrad Deetz, Bernhard Vogel

Karlsruhe Institute of Technology (KIT), Institute of Meteorology and Climate Research – Troposphere Research (IMK-TRO), Hermann-von-Helmholtz 1, 76344 Eggenstein-Leopoldshafen

HIGHLIGHTS

- Development of a new gas flaring emission parameterization for air pollution modeling.
- Combination of remote sensing observation and physical based combustion calculation.
- Application to the significant gas flaring region southern West Africa.
- Comprehensive assessing of the parameterization uncertainties.
- Comparison with existing gas flaring emission inventories.

Keywords:

Gas flaring
Emission parameterization
Emission uncertainty
Pollution modeling
Carbon dioxide

ABSTRACT

A new gas flaring emission parameterization has been developed which combines remote sensing observations using VIIRS nighttime data with combustion equations. The parameterization has been applied to southern West Africa, including the Niger Delta as a region which is highly exposed to gas flaring. Two two-month datasets for June-July 2014 and 2015 were created. The parameterization delivers emissions of CO, CO₂, NO and NO₂. A flaring climatology for both time periods has been derived. The uncertainties owing to cloud cover, parameter selection, natural gas composition and the interannual differences are assessed. Largest uncertainties in the emission estimation are linked to the parameter selection. ~~By using remote sensing cloud cover observations, a correction factor for the climatology was established to consider the effect of flares masked by clouds.~~ It can be shown that the flaring emissions in SWANigeria have significantly decreased by 3025% from 2014 to 2015. Existing emission inventories were used for validation. CO₂ emissions with the estimated uncertainty in brackets of ~~8 (±2/2.7 (3.6/0.5))~~ Tg y⁻¹ for 2014 and ~~5 (±1/2.0 (2.7/0.4))~~ Tg y⁻¹ for 2015 ~~are were~~ derived. ~~The flaring~~ Regarding the uncertainty range, the emission estimation within this study for June-July 2014 estimate is in the same order of magnitude compared to existing emission inventories. ~~For the same period in 2015 the emission estimation is one order of magnitude smaller in comparison to existing inventories, with a tendency for underestimation.~~ The deviations might be attributed to ~~uncertainties in a shortage in information about the derived flare gas flow rate combustion efficiency within southern West Africa,~~ the decreasing trend in gas flaring or inconsistent emission sector definitions. The parameterization source code is available as a package of R scripts.

1. Introduction

48 Gas flaring is a globally used method to dispose flammable, toxic or corrosive vapors to less reactive
49 compounds at oil production sites and refineries. In regions of insufficient transportation
50 infrastructure or missing consumers, flaring is also commonly applied.

51 CDIAC (2015a) estimated the global gas flaring emission of carbon dioxide to 267.7 million tons
52 (0.83% of total emissions) in 2008. Flaring and venting of gas significantly contributes to the
53 greenhouse gas emissions and therefore to the global climate change. The five countries with the
54 highest flaring amount in billion cubic ~~metermeters~~ (bcm) are Russia (35), Nigeria (15), Iran (10), Iraq
55 (10) and USA (5) (World Bank, 2012). These estimates were produced by National Oceanic and
56 Atmospheric Administration (NOAA) using Defense Meteorological Satellite Program (DMSP) remote
57 sensing data. Preliminary updates in global flaring estimates from NOAA for 2013 and 2014 are
58 available at http://ngdc.noaa.gov/eog/viirs/download_global_flare.html.

59 In recent time, especially with the development of remote sensing observation techniques (e.g.
60 Elvidge et al. (1997, 2013)), emissions from gas flaring moved in the focus of atmospheric research
61 involving the efforts in reducing the pollution and the waste of resources. The World Bank led the
62 initiatives “Global Gas Flaring Reduction Partnership” (GGFR) and “Zero Routine Flaring by 2030” to
63 promote the efficient use of flare gas.

64 Instead of relying on national statistics of gas production and consumption for estimating the flaring
65 amount, remote sensing techniques can estimate the flaring amount directly via multispectral data
66 (Elvidge et al., 2013). Elvidge et al. (2009) developed a 15 year dataset of global and national gas
67 flaring efficiency from 1994 to 2008 by using data from DMSP. Elvidge et al. (2015) presented
68 methods to derive global surveys of natural gas flaring using DMSP. For 2012 they have identified
69 7467 flares globally, with an estimated volume of flared gas of 143 (± 13.6) bcm. Doumbia et al.
70 (2014) combined DMSP with emission factors for flaring, to estimate the flaring emissions for SWA.
71 The satellite product Visible Infrared Imaging Radiometer Suite (VIIRS) Nightfire (Elvidge et al., 2013),
72 which is free available as “VIIRS Nightfire ~~Prerun V2.1 Flares only~~Nighttime Detection and
73 Characterization of Combustion Sources” (VIIRS, 2015) (~~VNP2015a~~) (VNF hereafter), is now the most
74 widely used product to derive flaring emissions from satellite imagery. By using ~~VNPVNF~~, Zhang et al.
75 (2015) estimated the methane consumption and the release of CO₂ from gas flaring for the northern
76 U.S. which agree with field data within an uncertainty range of $\pm 50\%$.

77 Also in the second largest flaring country Nigeria, the awareness of gas flaring increases. Nigeria
78 shows the fourth highest number of flare sites (approx. 300) worldwide after USA, Russia and Canada
79 (Elvidge et al., 2015). On gasflaretracker.ng the attention of the government, industry and society is
80 called to the flaring problem by interactive maps of flare infrastructure, amounts and costs. The
81 implications of gas flaring in Nigeria are far-reaching. It influences the environment by noise and
82 deterioration of the air quality (Osuji and Awiri, 2005). Nwankwo and Ogagarue (2011) have
83 measured higher concentrations of heavy metals in surface water of a gas flared environment in
84 Delta State Nigeria. Adverse ~~ecological~~ecological and bacterial spectrum modifications by gas
85 flaring are indicated by Nwaugo et al. (2006). Gas flaring also causes acid rain which causes economic
86 burden via rapid corrosion of zinc roofs (Ekpoh and Obia, 2010) and causes retardation in crop
87 growth owing to high temperatures (Dung et al., 2008).

88 The project DACCIWA (Dynamics-aerosol-chemistry-cloud interactions in West Africa, Knippertz et al.
89 (2015)) investigates the influence of anthropogenic and natural emissions on the atmospheric
90 composition over SWA, including the flaring hotspot Nigeria, to ~~examine~~quantify the ~~meteorological~~
91 ~~and socio-economic~~effects on meteorology and cloud characteristics. To consider the SWA gas
92 flaring emissions (e.g. in an atmospheric model), this study presents a method to derive emission
93 fluxes by combining the state of the art flaring detection ~~VNPVNF~~ and the combustion equations of

94 Ismail and Umukoro (2014) which does not use emission factors. The new parameterization is robust
95 and easy to apply to new research questions according flexibility in the spatiotemporal resolution.
96 The parameterization is presented in Section 2. Results of the application to SWA, including the
97 spatial distribution of gas flaring, the emission estimation and the uncertainty assessment are
98 investigated in Section 3. Section 4 places the emission estimates in the context of existing
99 inventories. The results are summarized and discussed in Section 5.

100

101 **2. Parameterization of gas flaring emissions**

102

103 The new parameterization for gas flaring presented here, is based on ~~VNP (VIIRS Nightfire Prerun~~
104 ~~V2.1 Flares only~~Nighttime Detection and Characterization of Combustion Sources (VNF hereafter)
105 and the combustion equations of Ismail and Umukoro (2014) (IU14 hereafter).

106

107 **2.1 Remote sensing identification of gas flares**

108

109 VIIRS (Visible Infrared Imaging Radiometer Suite) is a scanning radiometer for visible and infrared
110 light on board the sun-synchronous Suomi National Polar-orbiting Partnership weather satellite
111 (Suomi-NPP) (NASA, 2016). It can detect combustion sources at night (e.g. bush fires or gas flares) by
112 spectral band M10. To confirm these sources and to eliminate noise, the Day/Night Band (DNB), M7,
113 M8 and M12 are used in addition. By fitting these measured spectra to the Planck radiation curve,
114 background and source temperatures can be deduced. ~~VNP is filtered to include only detections with~~
115 ~~temperatures between 1600 K and 2000 K, which is believed to be an adequate estimation for~~
116 ~~average gas flares. Up to now no atmospheric correction is done (VIIRS, 2015 (VIIRS, 2015a)).~~

117 The data is freely available as daily cloud corrected data from March 2014 to present. The files
118 include among others the location of the flares combustion sources, source temperature T_s , radiant
119 heat H and time of observation.

120 VNF does not distinguish between the different combustion sources (e.g. wild fires or flaring). To
121 extract the flaring information from VNF a postprocessing is necessary. For this study we have

122 decided for a two month period of observation. This allows a compilation of a flaring climatology in
123 terms of the locations and emissions and a robust estimation of uncertainty owing to cloud coverage
124 and ~~other~~ parameters that have to be prescribed for IU14. We have selected the month June and July

125 because the gas flaring emission dataset will be used within the regional online-coupled chemistry
126 model COSMO-ART (Vogel et al., 2009) during the measurement campaign of the project DACCIWA,
127 which ~~takestook~~ place in June/July 2016. This campaign includes airborne, ground based and remote

128 sensing observations of meteorological conditions and air pollution characteristics. COSMO-ART is
129 one of the forecasting models of the DACCIWA campaign and delivers spatiotemporal
130 aerosol/chemistry distributions. The data for June/July 2014 and June/July 2015 are used to allow

131 also for an interannual comparison, and to assess the uncertainty owing to changes in flare processes
132 (e.g. built-up or dismantling, increase or decrease in combustion). The dataset includes the countries

133 which can affect SWA with their flaring emissions, in particular Ivory Coast, Ghana, Nigeria,
134 Cameroon, Gabon, Congo, the Democratic Republic of the Congo and Angola. The extraction of the

135 flaring information from the VNF data (VNF_{flare} hereafter) was realized by the Earth Observation
136 Group of NOAA. Within VNF_{flare} a csv file for every SWA flare is available, containing the flaring

137 history in June/July 2014 and 2015. For this study we use the location, source temperature and
138 radiant heat.

139 ~~For this study we use location, source temperature and radiant heat for days with sufficient satellite~~
 140 ~~coverage over the research domain SWA with a focus on the Niger Delta.~~
 141 ~~The authors want to point out that VNP delivers only a quick daily overview of global gas flaring~~
 142 ~~activity and is linked to uncertainties (e.g. flares in a single spectral band or with a source~~
 143 ~~temperature below 1400K cannot be detected). Instead of VNP, the original VIIRS files (available at~~
 144 ~~http://ngdc.noaa.gov/eog/viirs/download_viirs_fire.html) can be used as input for the~~
 145 ~~parameterization presented in this study but this requires a preprocessing to separate the flaring~~
 146 ~~sources from other combustion sources (e.g. wild fires).~~

148 2.2 Emission estimation method

149
 150 The principle emission estimation methodology used in this study follows IU14. The gas flaring
 151 emissions are estimated based on combustion equations for incomplete combustion including six
 152 flaring conditions given in Tab. 1. The equations are introduced in detail in IU14 and are therefore
 153 not presented here. This section concentrates on the application of the method of IU14 to the
 154 ~~VNP~~ $VNPVNF_{flare}$ data and the research domain ~~in~~ SWA.

155
 156 **Tab.1.** Reaction types for incomplete combustion of flared gas, depending on availability of sulfur in the flared gas and the
 157 temperature in the combustion zone which determines the formation of NO and NO₂.
 158

Reaction type	Sulfur in flared gas	Source temperature (K)	NO _x formation
1	No	< 1200	no
2	Yes	< 1200	no
3	No	$1200 \leq T_s \leq 1600$	only NO
4	Yes	$1200 \leq T_s \leq 1600$	only NO
5	No	> 1600	NO and NO ₂
6	Yes	> 1600	NO and NO ₂

159
 160 As input, IU14 needs the natural gas composition C of the fuel input of the flare, the source
 161 temperature T_s (temperature in the combustion zone), and the flare characteristics including
 162 combustion efficiency η (1 is complete combustion without Carbon monoxide formation) and
 163 availability of combustion air δ (above 1 ~~is means~~ excess and below 1 ~~is means~~ deficiency). In addition
 164 we need the flow rate F , the gauge pressure of the fuel gas in the flare p_g , and the fraction of total
 165 reaction energy that is radiated f . The value for f is estimated by averaging a table of literature
 166 values for f given in Guigard et al. (2000). The IU14 input is summarized in Tab. 2.

167
 168 **Tab.2.** Variables and parameters needed for IU14 or for deriving the fluxes of the air pollutants
 169

Parameter	Description	Reference	Unit
C	Natural gas composition	Sonibare and Akeredolu (2004)	%
T_s	Source temperature	VNP $VNPVNF_{flare}$ (VIIRS, 2015 <u>2015a</u>)	K
η	Combustion efficiency	0.8 (IU14)	-
δ	Availability of combustion air	0.95 (IU14)	-
H	Radiant heat	VNP $VNPVNF_{flare}$ (VIIRS, 2015 <u>2015a</u>)	MW
F	Flow rate	VNP $VNPVNF_{flare}$ (VIIRS, 2015 , TA-Luft (1986 <u>2015a</u>), (VDI 3782, 1985))	$m^3 s^{-1}$
p_g	Gauge pressure	34.475 (API, 2007)	kPa
f	Fraction of radiated heat	0.27 (Guigard et al., 2000)	-

170

171 The natural gas composition is taken from Sonibare and Akeredolu (2004). They have measured the
 172 molar composition of Nigerian natural gas in the Niger Delta area for ten gas flow stations. For this
 173 study we have calculated the average over these stations and merged the data according their
 174 number of carbon atoms (Tab. 3). H₂S fraction is rather low because it was detected only in two out
 175 of the ten flow stations.

176
 177 **Tab.3.** Molar composition of natural gas in Niger Delta (Nigeria) based on the measurements of Sonibare and Akeredolu
 178 (2004), averaged over ten flow station. The hydrocarbons are merged according to the number of C atoms.
 179

Constituent	Fraction (%)
Methan Methane (CH ₄)	78.47
Ethan Ethane (C ₂ H ₆)	6.16
Propane (C ₃ H ₈)	5.50
Butan Butane (C ₄ H ₁₀)	5.19
Pentane (C ₅ H ₁₂)	3.95
Hexane (C ₆ H ₁₄)	0.36
Carbon dioxide (CO ₂)	0.305
Nitrogen (N ₂)	0.06
Hydrogen sulfide (H ₂ S)	0.005

180
 181 The source Temperature T_s is taken from ~~VNPVNF~~_{flare}. The combustion efficiency η was set to 0.8 and
 182 the availability of combustion air δ to 0.95. IU14 remarked, that the reaction condition for flaring of
 183 $\eta \gg 0.5$ and $\delta \geq 0.9$ should be the norm in regions, where the effective utilization of this gas is not
 184 available or not economically. Strosher (2000) ~~indicate~~indicates a combustion efficiency of solution
 185 gas at oil-field battery sites between 0.62 and 0.82, and 0.96 for flaring of natural gas in the open
 186 atmosphere under turbulent conditions. EPA (1985) shows combustion efficiencies between 0.982
 187 and 1 for measurements on a flare screening facility. Section 3.3.2 will shed light on the uncertainty
 188 which arises from η and δ via a parameter sensitivity study. The authors strongly recommend a
 189 careful selection of η and δ since unrealistic combinations (e.g. higher combustion efficiencies with
 190 rather low availability of combustion air) can lead to negative NO and NO₂ emissions.

191 The flow rate, gauge pressure and fraction of radiated heat are not included in the parameterization
 192 of IU14 but are necessary to derive the mass emission rates which can be used as emission data for
 193 an atmospheric dispersion model.

194 The flow rate F (m³ s⁻¹) is ~~estimated by~~derived from Eq. 1 (~~TA-Luft, 1986~~VDI 3782, 1985)

$$F = M / (1.36 \cdot 10^{-3} (T_s - 283)), \quad (1)$$

$$F = M / (c_p (T_s - T_A)), \quad (1)$$

198
 199 where M is the heat flow in MW ~~and~~, c_p the mean specific heat capacity of the emissions, T_s the
 200 source temperature and T_A the ambient temperature. VDI 3782 (1985) provides a value of the mean
 201 specific heat capacity of
 202

$$c_p = 1.36 \cdot 10^{-3} \text{ MW s m}^{-3} \text{ K}^{-1} \quad (2)$$

203
 204 which is derived for a pit coal firing but VDI 3782 (1985) denotes, that this can be used for other flue
 205 gases as well since potential deviations are negligible. For the ambient temperature T_A we use
 206 298.15K as a fixed value, representative for the tropical region. Within a sensitivity study regarding
 207 the influence of T_A on the heat flow, we have used the averaged heat flow and source temperature

208 of all flares within the time period June/July 2015 and varied the ambient temperature between
 209 293K and 303K, as a reasonable temperature range in the tropical regions. The resulting maximum
 210 difference in the heat flow is 0.0036 m³ s⁻¹. Therefore we assume that the uncertainties using a fixed
 211 climatological value for the ambient temperature are negligible. For the application of this inventory
 212 to other regions the ambient temperature might be adapted. By using Eq. 1 and 2 the heat flow F can
 213 be derived as

$$F = M / (1.36 \cdot 10^{-3} (T_S - 298.15)), \quad (3)$$

215 with T_S in K.

217 We assume that the emitted heat flow M is equal to the total reaction energy of the flare.
 218 ~~VNP~~VNF_{flare} only detects the energy fraction that is radiated H and not the total energy M . By using
 219 the radiant heat H (observed by ~~VNP~~VNF_{flare}) and the factor f (fraction of H to the total reaction
 220 energy, Guigard et al., 2000), we estimate M as $H \cdot 1/f$. For the source temperature T_S we use the
 221 ~~VNP-observation~~VNF_{flare} observations.

222 The estimation of the fuel gas density, which is necessary to transform the flow rate F into an
 223 emission, is problematic due to the lack of data concerning the technical setup of the SWA flares. We
 224 assume that the dominating flare type is a low-pressure single point flare. Bader et al. (2011) pointed
 225 out that these flares are the most common flare type for onshore facilities that operate at low
 226 pressure (below 10 psi (69 kPa) above ambient pressure) and API (2007) remarks that most subsonic-
 227 flare seal drums operate in the range from 0 psi to 5 psi (34 kPa). Therefore we have decided for a
 228 gauge pressure p_g of 5 psi (34 kPa) above ambient pressure. Via Eq. 23 we can calculate the fuel gas
 229 density ρ_f

$$\rho_f = p_f / (R / (M_f T_a)), \quad (2)$$

$$\rho_f = p_f / (R / (M_f T_A)), \quad (3)$$

233 where p_f is the fuel gas pressure as the sum of ambient pressure (10.1325 kPa, taken as const) and
 234 gauge pressure p_g . R is the universal gas constant, M_f the molar mass of the fuel gas and ~~T_a~~ T_A the
 235 ambient temperature (~~293~~298.15 K, taken as const). Finally, the emission E (kg s⁻¹) of a species i is
 236 given by

$$E_i = \frac{m_i}{m_{total}} \rho_f F, \quad (34)$$

238 where m_i is the mass of the species i and m_{total} the total mass of the fuel gas, both delivered by the
 239 parameterization of IU14.

241 The combustion calculations within IU14 provide the species water, hydrogen, oxygen, nitrogen,
 242 carbon dioxide, ~~carbon~~monoxide, carbon dioxide, sulfur dioxide, nitrogen oxide and nitrogen
 243 dioxide. In the following only ~~CO, SO₂, NO and NO₂~~ the latter five are considered. However, no black
 244 carbon or volatile organic compounds (VOCs) are considered by IU14, although they are not
 245 negligible. Johnson et al. (2011) estimated the mean black carbon emission for a large-scale flare at a
 246 gas plant in Uzbekistan to be 7400 g h⁻¹ and Strosher (1996) measured the concentration of
 247 predominant VOCs 5 m above the gas flare in Alberta with 458.6 mg m⁻³. However, owing to the
 248 missing representation of black carbon and VOCs in IU14, these compounds are not considered in
 249 this study.

250 ~~A flaring emission comparison between several days or averaging over a certain period is problematic~~
251 ~~due to small variances in the VNP locations of the flares. This means even the same flare can be~~
252 ~~detected on a slightly different position the next day, which makes an emission averaging for every~~
253 ~~single flare difficult, especially in intensive flare areas. We bypass the problem by predefining a grid~~
254 ~~and allocating the flares to this grid. By using the source code written in R (R Core Team, 2013)~~
255 ~~delivered by this study, the user can define the grid size independently. For calculating the average~~
256 ~~over several days, the emissions for every single flare per day are calculated and summed up~~
257 ~~according to their belonging to a certain grid box. This leads to one big point source per grid box. The~~
258 ~~corresponding emissions are then averaged over the time period of interest for every grid box (flare~~
259 ~~box hereafter). Considering this approach within an atmospheric model, by selecting the same grid~~
260 ~~configuration for the flaring emission data and the model, no loss of information occurs.~~
261 By using the source code written in R (R Core Team, 2013) delivered by this study, the user can define
262 the grid size independently (e.g. model grid) on which the flaring point sources are allocated.

263

264 3. Results

265

266 3.1 Spatial distribution of gas flaring in SWA

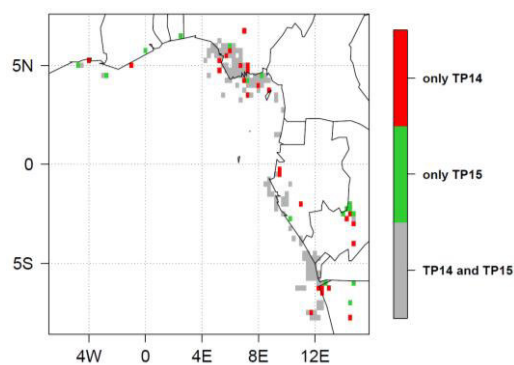
267

268 We have selected the two time periods June/July 2014 (TP14) and June/July 2015 (TP15) ~~and omitted~~
269 ~~all days without observations or with insufficient data coverage for VNP over SWA. This leads to 58~~
270 ~~(48) observations for TP14 (TP15) of VNF_{flare} over SWA (61 observations respectively).~~

271 In the preparation of this work we have compared the ~~estimated mean~~ locations of the flares of TP14
272 with the Google Earth imagery (Google Earth, 2014) (not shown). Only the onshore flares are visible
273 in Google Earth. This visual verification reveals that 72% of the ~~VNP~~ VNF_{flare} detected onshore flares
274 are visible in Google Earth. It is very likely that the hit rate is much higher since it is often the case
275 that the Google Earth image quality is not good enough for verification or the images are not up to
276 date. This comparison indicates that ~~VNP~~ VNF_{flare} is a valid and effective method to identify the flares in
277 SWA.

278 For the following analysis we have ~~calculated the emissions for both time periods on allocated the~~
279 ~~flares to~~ a grid with a mesh size of 0.25° (28 km) from ~~108~~ $^\circ$ S to ~~107~~ $^\circ$ N and from ~~105~~ $^\circ$ W to ~~1513~~ $^\circ$ E. ~~and~~
280 ~~calculated the emissions for both time periods. A grid box with flaring is denoted as flare box~~
281 ~~hereafter.~~ Fig. 1 emphasizes the areas in which ~~VNP~~ VNF_{flare} detects flares only in TP14 (TP15) in red
282 (green) color and in grey the areas with flaring in both periods.

283



284

285

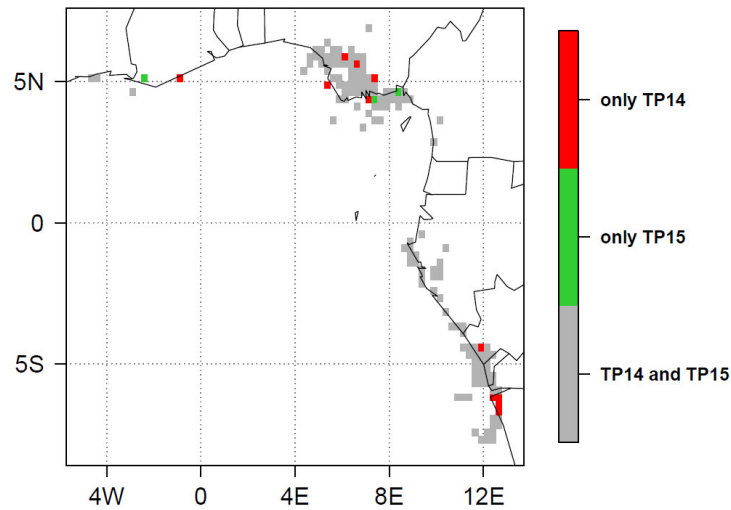


Fig.1. Flaring area for TP14 and TP15. Red (green) boxes denote areas with flaring only for TP14 (TP15). For the grey areas, flaring is detected in both time periods.

Remarkable are the dominating flaring areas in the Niger Delta and the adjacent offshore regions in the Gulf of Guinea. Also in the coastal region of Gabon, ~~Republic of the Congo~~, Angola and sporadically ~~along the coast in Ghana and offshore~~ of Ivory Coast, ~~Ghana and Benin~~, flaring occurs. By comparing TP14 and TP15 more red than green areas are visible, especially in southern Nigeria, which indicates a reduction in the flaring area from 2014 to 2015. The red areas contribute 12% to the total CO₂ emissions of TP14. VNF_{flare} detects 335 flares in 2014 and 312 flares in 2015 which means a reduction of about 7% (counted are those which deliver at least once a value for T_s and H in the time period). 61% of that reduction is related to Nigeria. A decrease in CO₂ from 1994 to 2010, particularly in the onshore platforms is indicated by Doumbia et al. (2014).

Fig. 2 shows the density of flares (a) and the flaring activity (b) per flare box for TP15. The results are similar to TP14, therefore only the TP15 is displayed here.

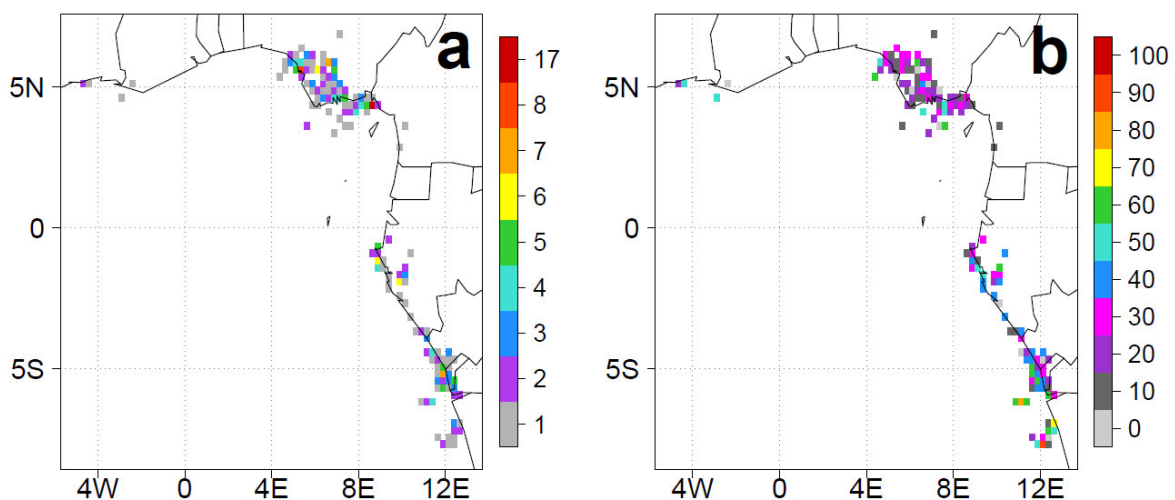
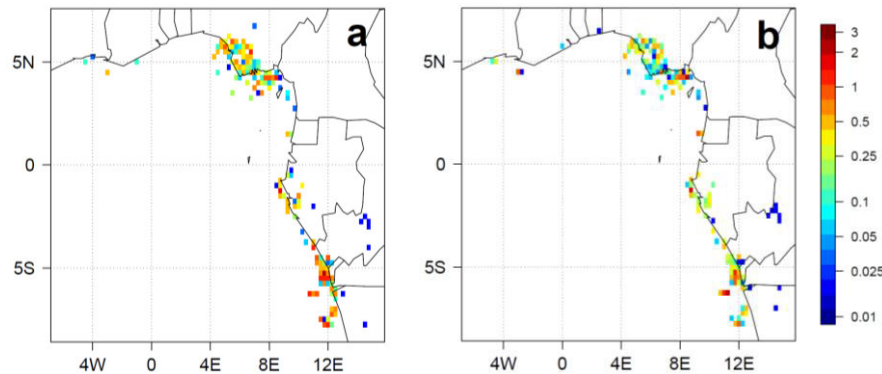


Fig.2. (a) Number of flares per flare box and (b) flaring activity (%) per flare box within TP15. A flaring activity of 100% means that every day on the 61 day period in June/July flaring was detected.

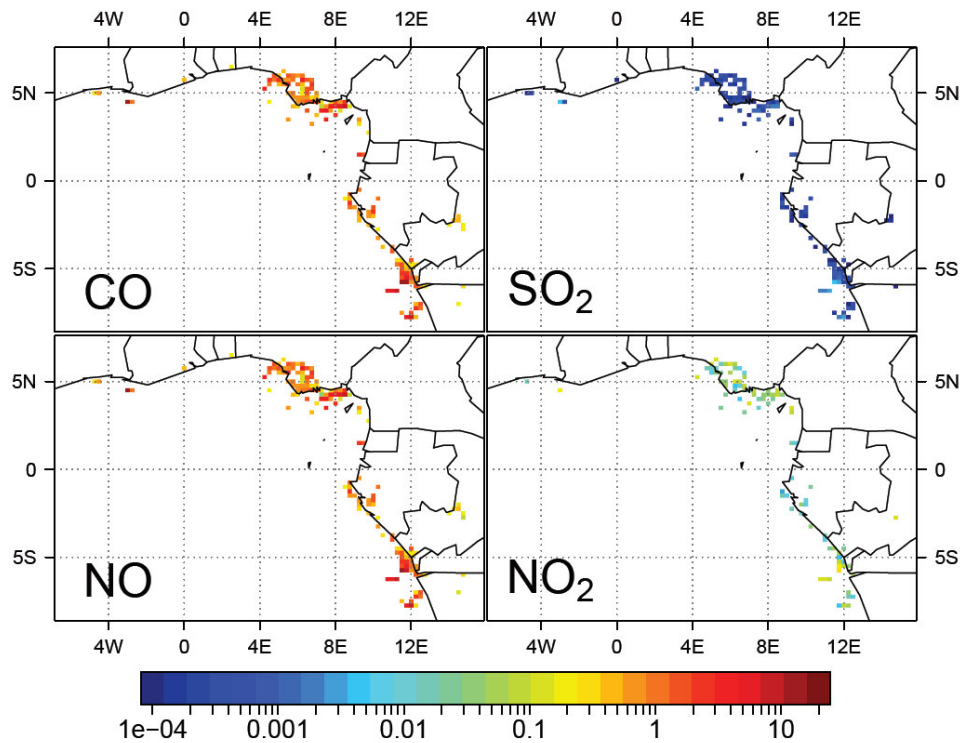
308 The highest flare density can be found offshore in the border area of Nigeria and Cameroon with 17
 309 flares per flare box. The offshore flaring density is smaller than onshore (Fig. 2a) whereas the highest
 310 flaring activity can be found offshore (Fig. 2b). The mean active flare density, as the sum over all
 311 detected flares in a box averaged over the time period, is shown in This could be linked to the
 312 increased masking of flares by clouds over land. The large onshore flaring area of the Niger Delta
 313 shows a comparable low flaring activity of 10-30%. Highest values can be found offshore of the
 314 Democratic Republic of the Congo and Angola of 50-90%. How the interannual variability of flaring
 315 reflects in the amount of flaring emissions is analyzed in section 3.3.4.
 316 Fig. 2 for (a) TP14 and (b) TP15.
 317



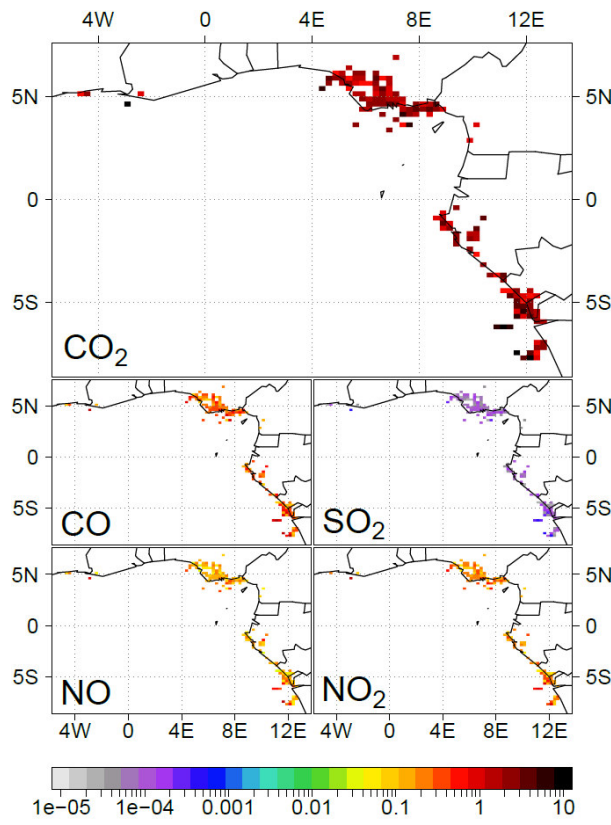
318 Fig. 2. Mean active flare density (number of active flares per box) averaged over (a) TP14 and (b) TP15 in logarithmic scale
 319
 320
 321 Fig. 2 shows to a a reduction in the active flare density in TP15 compared to TP14. 72% of the flaring
 322 area which TP14 and TP15 have in common, shows a reduction in TP15 about 48% on average. 28%
 323 of the common flaring area shows an increase in TP15 about 124%. Therefore it seems that the
 324 flaring intensity decreases in TP15 over large areas but simultaneously some flaring hotspots
 325 occurred, which are distributed along the SWA coast (not shown). Fig. 2, together with the variation
 326 of flaring emissions from TP14 to TP15 in Section 3.3.3, indicates the high year to year variations. This
 327 makes the use of past averaged conditions questionable, especially when certain episodes are
 328 studied.
 329

330 3.2 Emission estimation

331
 332 For the emission estimation we have used a climatological approach (E_{clim}). For every day with valid
 333 data in TP14 and TP15 the emissions for all detected flares are calculated separately and allocated to
 334 the predefined grid. The emissions are summed up in every flare box to have one joined flare per grid
 335 box. Finally the temporal average for every grid box is calculated averages of source temperature and
 336 radiant heat over TP14 and TP15 respectively were used to calculate the emissions. Therefore in this
 337 approach all flares, detected in the time period, are active at once with their mean emission
 338 strength. This method has the advantage that most likely all flares in the domain are captured even if
 339 a fraction of them is covered by clouds at certain days. However, this could lead to an emission
 340 overestimation because not all available flares are active at once. This problem of separating
 341 between flares which are not active and flares which are active but covered by clouds and therefore
 342 not visible for $VNPVNF_{flare}$ is picked up again in Section 3.3.1. Fig. 3 shows the emissions of CO_2 , CO,
 343 SO_2 , NO and NO_2 in $t\ h^{-1}$ for TP15.
 344



345



346

347

348 **Fig.3.** Flaring emissions for TP15 within E_{clim} in t h^{-1} for considering CO_2 , CO, SO_2 , NO and NO_2 . For better visibility the
 349 emissions are displayed as colored grid boxes although the emissions are still point sources and not area sources.

350

351 Highest emissions are ~~calculated~~derived for carbon ~~monoxide~~dioxide, followed by carbon monoxide,
 352 nitrogen dioxide and nitrogen dioxide. Sulfur dioxide shows lowest emissions since these
 353 emissions do not depend on combustion processes but only on the natural gas composition (see Tab.
 354 3) and the amount of flared gas (IU14). Due to the use of the averaged measurements of Sonibare

355 and Akeredolu (2004), local variations of hydrogen sulfide concentrations in the natural gas cannot
356 be taken into account. Hydrogen sulfide is the only source of sulfur in the flared gas and therefore
357 determines the emission of sulfur dioxide. To assess this uncertainty, a sensitivity study with
358 different hydrogen sulfide concentrations is given in Section 3.3.5.

359

360 3.3 Estimation of uncertainties

361

362 In the following section the most relevant uncertainties are presented, together with approaches for
363 their assessment. This includes the uncertainty concerning the flare detection in the presence of
364 cloud cover, the uncertainty in the determination of the emitted heat flow H via the fraction of
365 radiated heat f , the uncertainty in the choice of the IU14 parameters and the changes in flare
366 operation from one year to another as well as the influence of the spatial variability of hydrogen
367 sulfide in the natural gas on the sulfur dioxide emissions. Apart from Section 3.3.4 all uncertainty
368 estimations are confined to TP15.

369

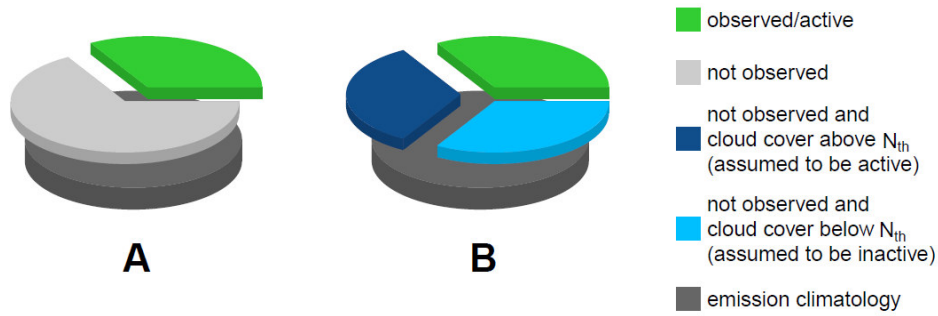
370 3.3.1 Uncertainty due to cloud cover

371

372 In this section we want to estimate the emission error due to cloud-covered flares and present a
373 method to derive daily emissions by considering the contribution of these masked flares. In Section
374 3.2 a climatological data set of flaring emissions (E_{clim}) was derived. ~~When using this data set we, in~~
375 which all available flares are losing the active with their mean emission strength. This dataset
376 therefore does not include a day to day variation of the flaring emissions that. If an emission dataset
377 with a daily variability is delivered by VNP. Although daily satellite observations are
378 available required, the problem arises that usually parts of the scene observed by the satellite are
379 covered by clouds. ~~In and therefore the following we will describe a method of how to derive daily~~
380 flaring emissions based on are likely underestimated. VNF_{flare} includes the climatological emissions
381 (E_{clim}), a threshold of cloud coverage (N_{th}), and locations of all flares independent whether there are
382 active or not. This entity is illustrated by the actual detected flares closed dark grey pie in Fig. 4A and
383 4B. By comparing the flares which are observed/active at a certain day. This is illustrated
384 schematically by Fig. 4. and the total

385 ~~The closed grey pie in the lower layer of Fig. 4A gives the climatological number of flaring boxes in~~
386 flares, a separation between observed (green pie in Fig. 4A) and not observed (light grey pie in Fig.
387 4A) is possible. In addition VNF_{flare} delivers a cloud mask for all of the research domain. At a certain
388 day only within flare detections. Therefore it is possible to separate the green flaring boxes active
389 flares are detected by VNP. The flaring boxes that are indicated in grey are those at which no active
390 flares were detected by VNP, either because they are light grey pie of the not observed flares in (a)
391 cloud-free and inactive or obscured by clouds. We now further separate this grey area by introducing
392 an empirical threshold value N_{th} of cloud cover. In areas that belong to the grey fraction in Fig 4A,
393 where the cloud cover is above N_{th} , we assume that the flares boxes are active and emit with their
394 climatological emission values (since there are no current observations available). Those flare boxes
395 are indicated by the dark blue color in Fig 4B. The light blue area indicates flare boxes where the
396 cloud cover is below N_{th} and where no flares are detected by VNP. For this area we postulate that all
397 flare boxes are inactive and consequently have zero emissions. Finally we calculate the total
398 emissions at a certain day for $N_{\text{th}}=50\%$ (E_{50}), 75% (E_{75}) and 90% (E_{90}) as the sum of the climatological
399 emissions in the dark blue area and the directly detected flares in the green area. (light blue pie in
400 Fig. 4B) and (b) cloud-covered and unknown flaring status (blue pie in Fig. 4B).

401



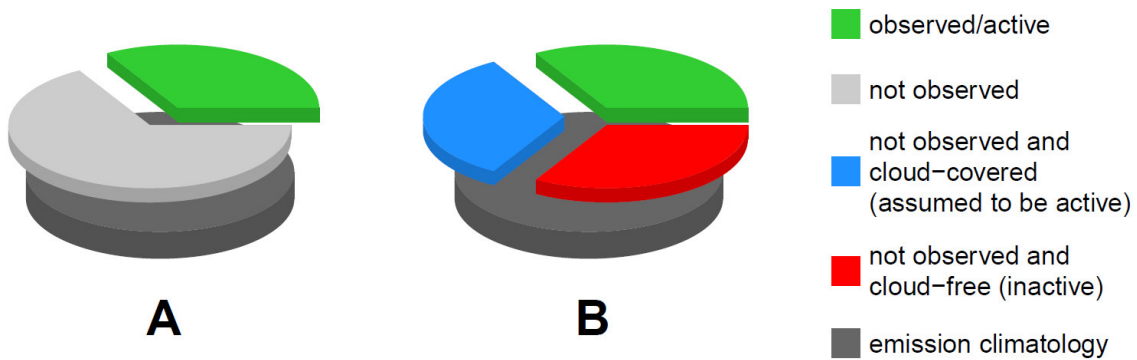
402

403

404

405

To estimate the error due to active but cloud-covered flares, we assume that all of these flares are active with their mean emission strength observed in June/July 2015.



406

407

408

409

410

411

412

413

414

415

416

417

Fig.4. Pie charts illustrating the flaring emission uncertainty assessment due to cloud cover for TP15. The ~~entirety~~entity of the ~~flare boxes~~flares within the emission climatology (E_{clim}) is given as closed grey pie in the bottom of **A** and **B**. **A** distinguishes between ~~flare boxes in which~~ flares which are detected/active at a certain day (green) and the complement of undetected ~~flare boxes~~flares (light grey). In **B** the light grey slice of **A** is separated in a cloud-covered (~~above cloud cover threshold N_{th}~~ , dark blue) and cloud-free (~~below N_{th}~~ , light blue)red part by using ~~remote sensing observations~~. Flare ~~boxes~~the cloud mask of VNF_{flare} . Flares which are not detected by $VNPVNF_{flare}$ and ~~simultaneously show a cloud cover above N_{th}~~ covered by clouds are taken as active. Flare ~~boxes~~Flares which are not detected by $VNPVNF_{flare}$ and ~~simultaneously show a cloud cover below N_{th}~~ are not covered by clouds are taken as inactive. For N_{th} , the values 50%, 75% and 90% are used. The higher N_{th} , the smaller the dark blue slice in **B**.

418

419

420

421

422

423

424

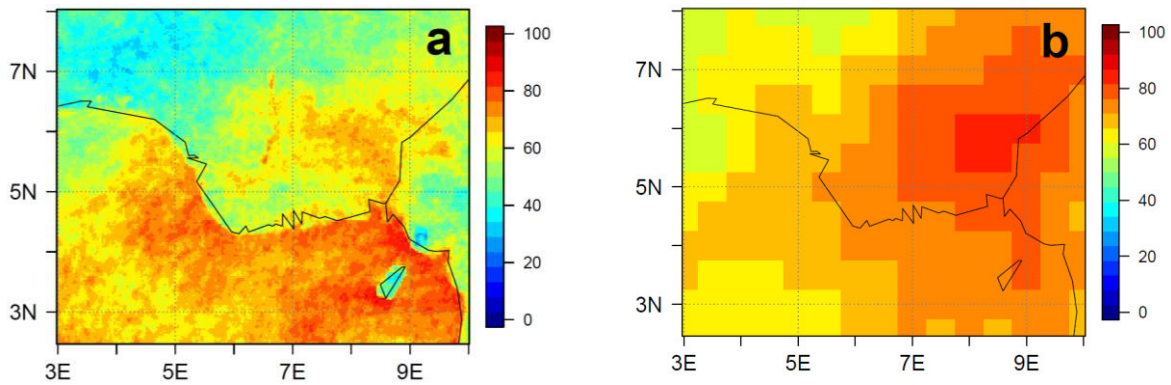
425

426

427

Fig. To separate the light grey slice in Fig. 4A in covered and uncovered flare boxes, we used 5 illustrates the mean cloud cover exemplarily for the greater Niger Delta area using (a) instantaneous cloud fractional cover (CFC) from the geostationary Meteosat Second Generation 3 (MSG3) (CM SAF, 2015, copyright (2015) EUMETSAT) for every day of TP15 around the time of $VNPVNF$ observation (Suomi-NPP overflight approx. at 1 UTC). This method is applied to all days of TP15 for every flare ~~box~~ and (b) the sun-synchronous Aqua/AIRS (Mirador, 2016).

To ensure a consistent timing between cloud observation and VNP observation, the spatial domain was reduced with a focus on the Niger Delta area (see Fig. 5a) and the flares were allocated according to the cloud data grid with a mesh size of 0.03° .

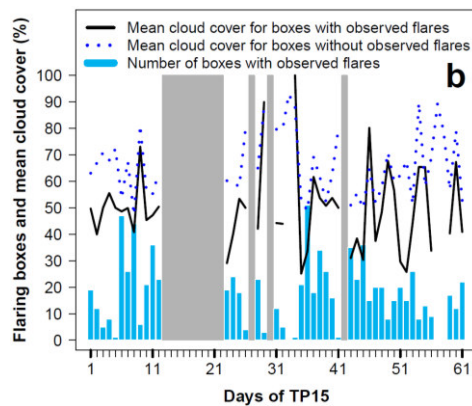


428
429 **Fig.5.** Fractional cloud cover (%) observed from (a) the geostationary MSG3 and (b) the sun-synchronous Aqua/AIRS,
430 averaged over TP15 around the time of ~~VNP/VNF~~ observation (approx. 1 UTC).
431

432 Fig. 5a shows that the onshore flaring area for TP15 is in mean covered with clouds by 50-70%. For
433 the offshore flaring area it is even higher with 70-90%. Therefore it is very likely that flares are
434 frequently masked by clouds and therefore not detected by ~~VNP/VNF~~. However, we suspect that the
435 MSG3 cloud product underestimates (overestimates) the onshore (offshore) cloud cover when
436 comparing with the findings of van der Linden et al. (2015). The high offshore coverage and the
437 distinct land-water separation might be caused by overestimating low clouds in the presence of a
438 warm and moist tropical ocean.

439 Fig. 5b shows a cloud climatology using Aqua/AIRS Nighttime data (Mirador, 2016). The Aqua/AIRS
440 climatology shows higher cloud cover over land and no distinct separation between water and land
441 surface. Both products identify the highest onshore cloud cover in the northeast of Port Harcourt
442 (4.8°N, 7.0°E) and have similar values in the Nigerian offshore region (containing the offshore flares)
443 of about 70-80%. The major difference in the climatologies appears onshore between 4.5°N and 6°N.
444 This area includes the majority of the Nigerian onshore flares. ~~Although it is not the aim of this study
445 to identify the most reliable cloud climatology for SWA, it has to be considered that MSG3 likely
446 underestimates the mean cloud cover over the Nigerian onshore flares up to 30%. This reveals a
447 relatively high uncertainty in the estimation of nocturnal low cloud coverage from remote sensing.
448 However, in the following the cloud climatology derived from MSG3 (Fig. 5a) is used since Aqua/AIRS
449 cannot provide the full spatial coverage for every day (due to the sun-synchronous orbit of
450 Aqua/AIRS).~~

451



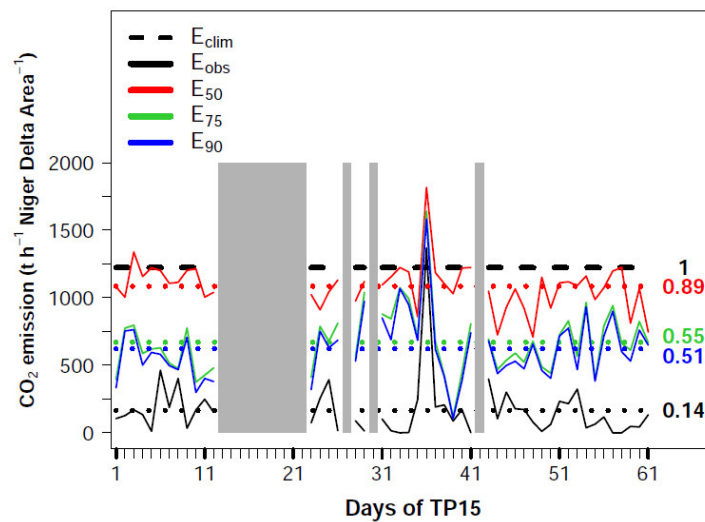
452
453 **Fig.6** Number of boxes with detected flares per day (blue bars) and the mean fractional cloud cover for the boxes with
454 (without) detected flares as black solid (blue dotted) line (using MSG3, compare Fig. 5a). For the calculation of the latter,
455 the cloud cover of the non-active flare boxes within E_{clim} are averaged (compare Niger Delta area in Fig. 2b). ~~The grey
456 shaded areas are omitted due to lack of VNP observation.~~
457

458
459
460
461
462
463
464
465
466
467
468
469
470
471
472
473
474
475
476
477
478
479
480
481
482
483

Fig. 6 shows the number of grid boxes with active flares per day in TP15 as, separated in the categories: cloud-free/active (green), cloud-free/inactive (red) and cloud-covered (blue bars. The grey areas indicate). Flares with no or incomplete data gaps are coded in VNP black. E_{clim} includes 185 flare boxes according to the domain in Fig 5a. For TP15 not more than 51 flare boxes are detected at once. In 312 flares which are at least once active in TP15. On average only 826% of the total flaring area is active at once. As expected the temporal evolution of the flare boxes and the, 9% is verifiable inactive and 63% is cloud-cover for these boxes (black solid line in Fig. 6) shows an anticorrelation. The highest number of flare boxes at day 36 is reached in a period of a comparatively low cloud cover. The mean cloud cover for the non-active flare boxes of E_{clim} (blue dotted line in Fig. 6), is in general higher than for the active flare boxes which implies that the cloud cover reduces the VNP detections. Fig. 6 also reveals that it is not suitable to use the strict cloud free condition for the separation in Fig. 4B because nearly all of the boxes would be assigned to the dark blue cloud covered fraction and the resulting emissions would be nearly the same as E_{clim} . However, it has to be considered that the light points of flares are extremely small-scale signals (1/5000 of the VNP pixel, Zhang et al. (2015)) and even for an almost completely closed cloud deck VNP detections are possible.

The climatology E_{clim} is the reference for this study. In addition we define E_{obs} which only considers the actually observed flares per day. E_{50} is defined as the combination of actually observed flares and cloud covered flares (see Fig. 4) with a. By taking into account only the cloud cover threshold-free information instead of 50%. E_{75} (E_{90}) is equal to E_{50} but uses a cloud cover threshold the climatological approach of 75% (90%).

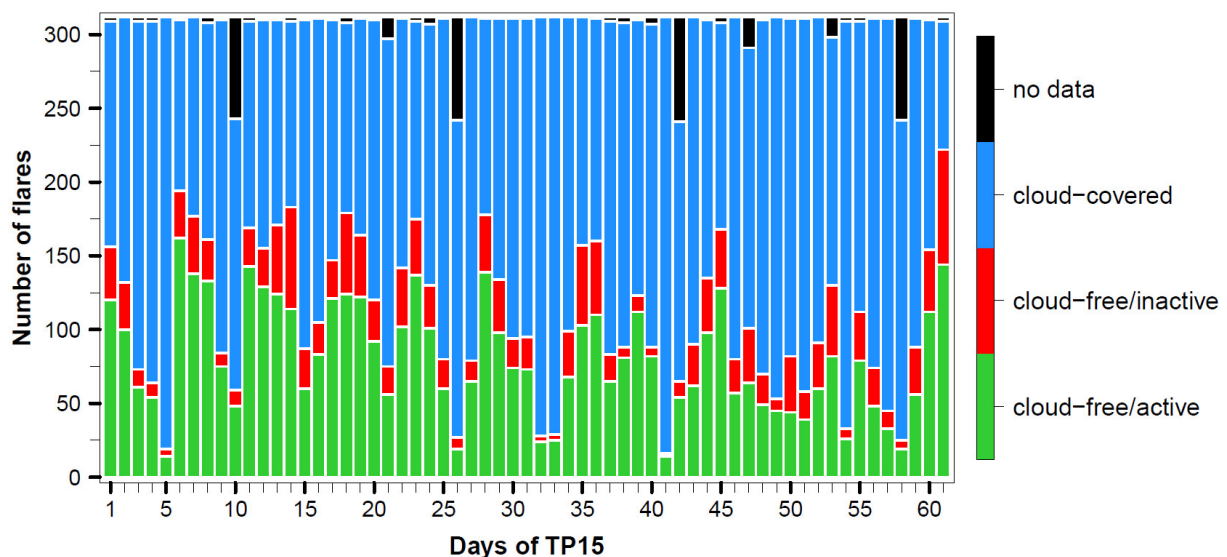
To emphasize the difference between the different emission estimates, Fig. 7 shows the daily emissions of CO_2 for TP15 as a spatial sum over the Niger Delta area (see Fig. 4a). In contrast to E_{clim} (black dashed line), E_{obs} , E_{50} , E_{75} and E_{90} (solid lines) have a temporal variation within TP15.



484
485
486
487
488
489
490
491
492

Fig. 7. Daily CO_2 emissions ($kg\ h^{-1}$) within TP15 from flaring summed up over the Niger Delta area defined in Fig. 4a for the five emission estimates: E_{clim} (climatology, black dashed line), E_{obs} (VNP observations, black solid line), E_{50} (combination of VNP observations and the climatology for a cloud cover threshold of 50%, red solid line), E_{75} (as E_{50} but for a cloud cover threshold of 75%, green solid line), E_{90} (as E_{50} but for a cloud cover threshold of 90%, blue solid line). The dotted lines denote the spatiotemporal, on average of E_{obs} , E_{50} , E_{75} and E_{90} . The numbers on the right hand side show the ratios of the spatiotemporal averages E_{obs} , E_{50} , E_{75} and E_{90} towards E_{clim} . The grey shaded areas are omitted due to lack of VNP observation.

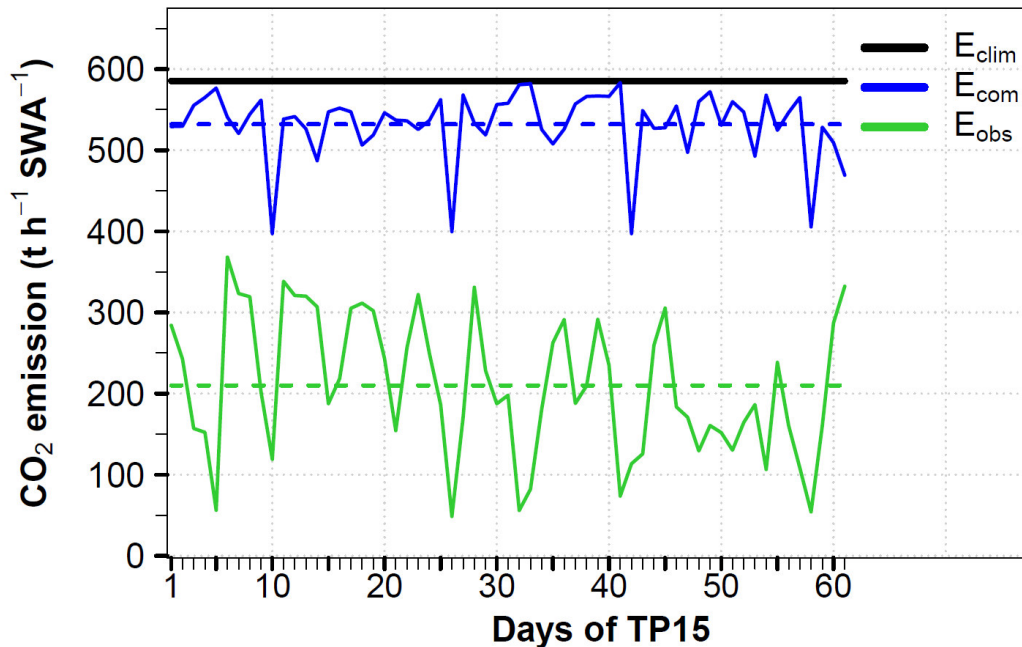
493 E_{clim} delivers a daily CO_2 emission of about 1250 t h^{-1} within the Niger Delta area. The pure daily VNP
 494 observations within E_{obs} (black solid line) show only 14% of E_{clim} emissions (numbers on left hand side
 495 of Fig. 7) on average (black dotted line). The emissions from VNP observations together with the
 496 climatology for the cloud threshold of 50% within E_{50} (red solid line) is closest to the climatology (89%
 497 of E_{clim} , red dotted line). The high overall cloud cover within the domain (compare with blue dotted
 498 line in Fig. 6) together with the relative low cloud cover threshold leads to the result, that nearly the
 499 complete climatology is used for E_{50} and therefore the difference to E_{clim} is small. The emissions from
 500 VNP observations together with the climatology for the cloud threshold of 75% and 90% within E_{75}
 501 and E_{90} (green and blue solid line) shows only small deviations but are significantly reduced in
 502 comparison to E_{clim} (55% and 51% of E_{clim} , green and blue dotted line). Day 36 of TP-15 shows highest
 503 emissions in E_{obs} , E_{50} , E_{75} and E_{90} , owing to the combination of low cloud cover and high flaring
 504 activity (compare with Fig. 6). Regarding the uncertainty in the cloud cover climatology (compare Fig.
 505 5a and Fig. 5b), the emissions of E_{50} , E_{75} and E_{90} might be underestimated. The 63% of the flares are
 506 not considered at a certain day. By assuming that all of these cloud-covered flares are active, a
 507 remarkable underestimation of the cloud cover in the onshore flaring area could lead to an
 508 unjustified increase in flare boxes below N_{th} and therefore to a reduced number of active flares per
 509 day can be expected.



511 **Fig.6.** Number of flares per day in TP15 which are cloud-free and active (green), cloud-free and inactive (red) and cloud-
 512 covered (blue). Flares with no or incomplete data are denoted in black. The color coding follows Fig. 4B. Considered are the
 513 312 flares which deliver at least once a value for T_s and H in TP15.

514 In addition to E_{clim} two further emission inventories are introduced: E_{obs} only considers the actual
 515 daily observed flares (linked to the green flares in Fig. 6). To consider also the contribution of active
 516 but cloud-covered flares, E_{com} combines the green and the blue flares of Fig. 6.
 517 To allow for consistency, all three inventories use the emissions derived from the flare specific
 518 temporal averages of the source temperature and the radiant heat over TP14 and TP15 respectively.
 519 We avoid calculating the emissions from instantaneous source temperatures because this is linked to
 520 high uncertainty depending on the atmospheric conditions (Mikhail Zhizhin, personal
 521 communication). The temporal averages allow for robustness. Therefore the three inventories only
 522 differ in the selection of the active flares per day but not in the underlying emissions. E_{clim} uses all
 523 flares at a certain day, E_{obs} considers only the flares which are cloud-free and active and E_{com}

527 considers E_{obs} plus the cloud-covered flares, by assuming that all of the cloud-covered flares are
 528 active. Nevertheless we have included a further inventory in Tab. 5 which uses instantaneous source
 529 temperature and radiant for the emission derivation (E_{clim} , instant. input) to assess the differences
 530 towards the averaged input. Fig. 7 shows the total CO_2 emissions of the SWA area from E_{clim} in black,
 531 from E_{obs} in green and from E_{com} in blue.
 532



533 **Fig.7.** Daily CO_2 emission estimations ($t h^{-1}$) within TP15 from flaring, summed up over the SWA area as denoted in Fig. 1 for
 534 the three emission inventories: E_{clim} (climatology, black solid line), E_{obs} (daily VNF_{flare} observations, green solid line and
 535 temporal average as green dashed line) and E_{com} (sum of daily VNF_{flare} observations and emissions from cloud-covered
 536 flares, blue solid line and temporal average as blue dashed line). The periodical drop of the blue line is linked to reduced
 537 data coverage (compare with black bars in Fig. 6).
 538
 539

540
 541 The dashed lines denote the temporal averages of E_{obs} and E_{com} . On average E_{com} is only 9% smaller
 542 than E_{clim} which is assumed to be in the range of uncertainty. Therefore both inventories are
 543 equitable in this study. The user can decide whether a temporal resolved or a climatological
 544 approach fits best to their research question.

545 The emissions of E_{obs} are strongly reduced (64%) compared to E_{clim} as expected. The use of E_{obs} would
 546 significantly underestimate the emissions and is therefore not appropriate for an application. Since
 547 E_{obs} does not take into account cloud-covered flares at all and E_{com} in contrast sees all cloud-covered
 548 flares as active, the difference between these inventories can be used to assess the uncertainty
 549 arising from flares masked by clouds. Fig. 7 shows a mean difference between E_{obs} and E_{com} of about
 550 61%. Therefore while using E_{obs} as a flaring emission inventory in an application, an underestimation
 551 of the emissions of 61% has to be considered.

552 These emission estimations contain different information. E_{clim} includes all flares of the domain
 553 despite cloud-coverinvariant but can overestimate the emissions. E_{obs} shows the $VNPVNF_{flare}$ reality,
 554 including a temporal development, but cannot consider the cloud-covered flares. ~~E_{507} , E_{75} and E_{90}~~
 555 ~~combine~~ E_{com} combines the flare location climatological information of E_{clim} for flares which are not
 556 observable at a certain time and the full temporal resolution of $VNPVNF_{flare}$ in E_{obs} by using cloud
 557 observations. However this approach is based on the assumption that all cloud-covered flare boxes
 558 are active, which is also linked to high uncertainty. Additionally E_{507} , E_{75} and E_{90} depend on the

559 availability of a longer VNP observational dataset. The ratios of the spatiotemporal means of E_{obs} , E_{50} ,
 560 E_{75} and E_{90} to the spatial mean of E_{clim} (as denoted by the numbers in Fig. 7) are used as correction
 561 factors (CF) for E_{clim} in the following (see Tab. 4). E_{clim} is taken as the reference (CF=1).

562
 563 **Tab.4.** Emission estimations including information about flaring (daily observation and climatology) and cloud cover
 564 observation. The correction factors (CF) are derived for TP15 from a spatiotemporal emission mean in the Niger Delta area
 565 (2.5°N-8°N, 3°E-10°E) and refer to E_{clim} .

Name	Emission estimate	CF for E_{clim}
E_{clim}	Climatology (reference)	1
E_{obs}	Observed flares	0.14
E_{50}	Observed flares + climatology ($N_{\text{th}}=50\%$)	0.89
E_{75}	Observed flares + climatology ($N_{\text{th}}=75\%$)	0.55
E_{90}	Observed flares + climatology ($N_{\text{th}}=90\%$)	0.51

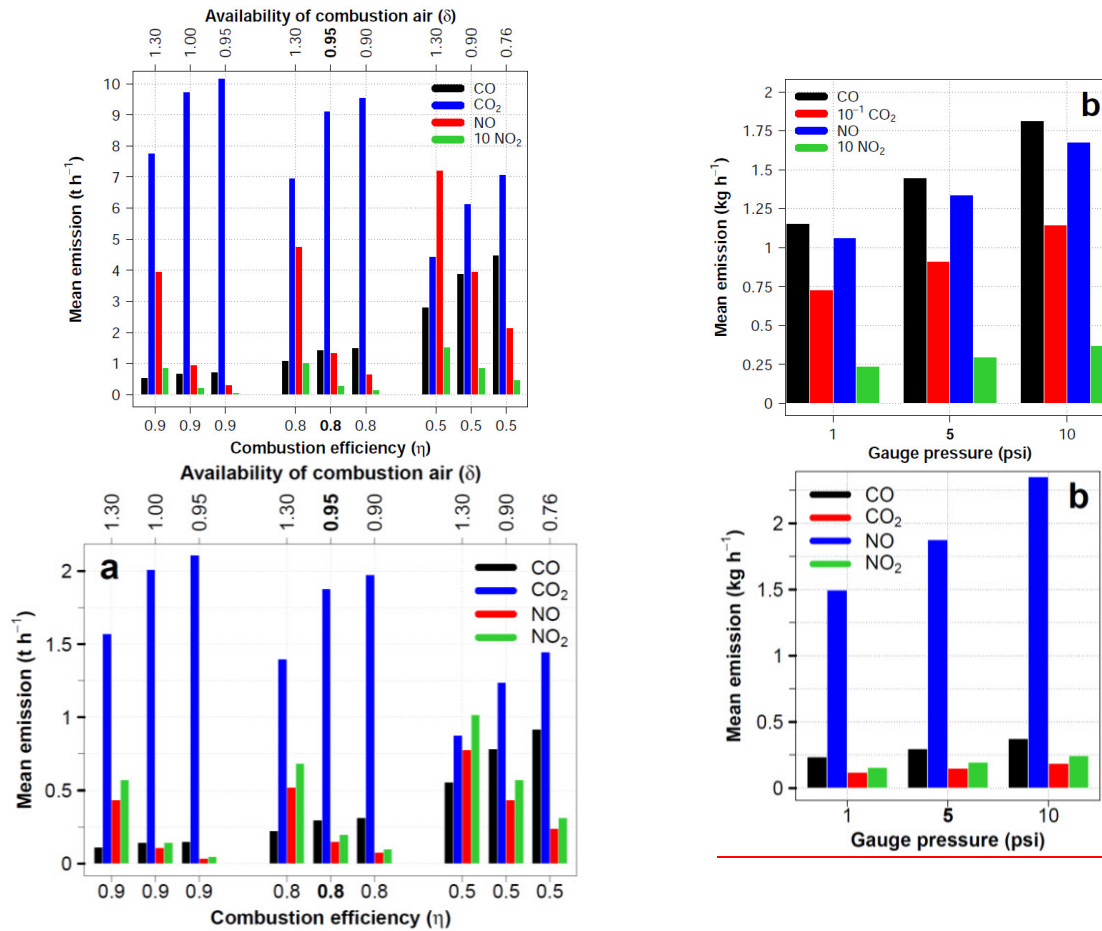
567
 568 These CF are a simple method to include the information of E_{obs} , E_{50} , E_{75} and E_{90} into E_{clim} by
 569 multiplying E_{clim} with the corresponding correction factor. In this case the same 185 flare boxes of
 570 E_{clim} are used but with an emission strength reduced to the averaged conditions of E_{obs} , E_{50} , E_{75} and
 571 E_{90} . This approach is based on the assumption that the correction factor, deduced for the Niger Delta
 572 area, is valid for the whole domain specified in Section 3.1. This assumption seems to covered flares
 573 are active, which can be justified since the Niger Delta area contains seen as an estimation upwards.
 574 Therefore the most of the gas flares in the domain likely amount of emissions is expected between
 575 E_{obs} and E_{com} .

577 3.3.2 Uncertainty due to IU14 input parameters

578
 579 To assess the uncertainty which arises from the combustion efficiency η and the availability of
 580 combustion air δ , a sensitivity study has been carried out. The exact values for the SWA flares are
 581 unknown and very likely highly variable from one flare to another, depending on the flare type and
 582 operation. Fig. 8a shows the flareflaring emissions averaged over SWA and TP15 for CO, CO₂, NO and
 583 NO₂. The parameters η and δ are varied referring to IU14. A complete combustion ($\eta = 1$) does not
 584 produce CO emissions since all carbon is transformed to CO₂ (not shown). With decreasing η and δ ,
 585 the CO and CO₂ emissions increase. Concerning CO we assume the lower limit for $\eta = 0.9$ and
 586 $\delta = 1.3$ (left of Fig. 8a) and the upper limit for $\eta = 0.5$ and $\delta = 0.76$ (right of Fig. 8a). The values
 587 used for this study are located in the center of Fig. 8a-8a (printed in bold). By taking the latter as
 588 reference, the lower (upper) limit leads to a decrease (increase) in CO emission of -63% (+210208%).
 589 For CO₂ we derived an lower (upper) limit of +38% (-72-53% (+12%).

590 A higher combustion efficiency or a higher availability of combustion air allows an enhanced
 591 formation of NO and NO₂. Therefore NO_x emissions increase (decrease) with decreasing η . In
 592 contrast these emissions decrease with an increase in the combustion efficiency (δ). The higher the
 593 efficiency the more oxygen is forming CO₂ instead of NO_x. We assume the lower limit for $\eta = 0.9$ and
 594 $\delta = 0.95$ and the upper limit for $\eta = 0.5$ and $\delta = 1.30$. Taking again the central parameter set of Fig.
 595 8a as reference, the lower (upper) limit leads to a decrease (increase) in NO emission of -77%
 596 (+44176% (+420%).

597



598
 599 **Fig.8.** Flaring emissions (kg h^{-1}) spatiotemporally averaged over SWA and TP15 depending on (a) combustion efficiency η
 600 and availability of combustion air δ for a gauge pressure of 5 psi and (b) gauge pressure (psi) for the setup of $\eta = 0.8$ and δ
 601 which is used for this study (emphasized in bold), $= 0.95$. SO_2 is not shown because it does not depend on η or δ .

602
 603 ~~The emissions of NO_2 are comparatively low owing to the source temperature which is in general~~
 604 ~~lower than the NO_2 formation threshold of 1600 K.~~

605 ~~For NO_2 the emission decrease (increase) is -76% (+417%).~~

606 In addition, Fig. 8b shows the emissions depending on the gauge pressure for 1 (lower limit), 5 and
 607 10 psi (upper limit) (7, 34 and 69 kPa respectively) for $\eta = 0.8$ and $\delta = 0.95$. Regarding Using 5 psi as
 608 the reference, the lower (upper) limit leads to a decrease (increase) in CO emissions of -21% (+2620%
 609 +25%).

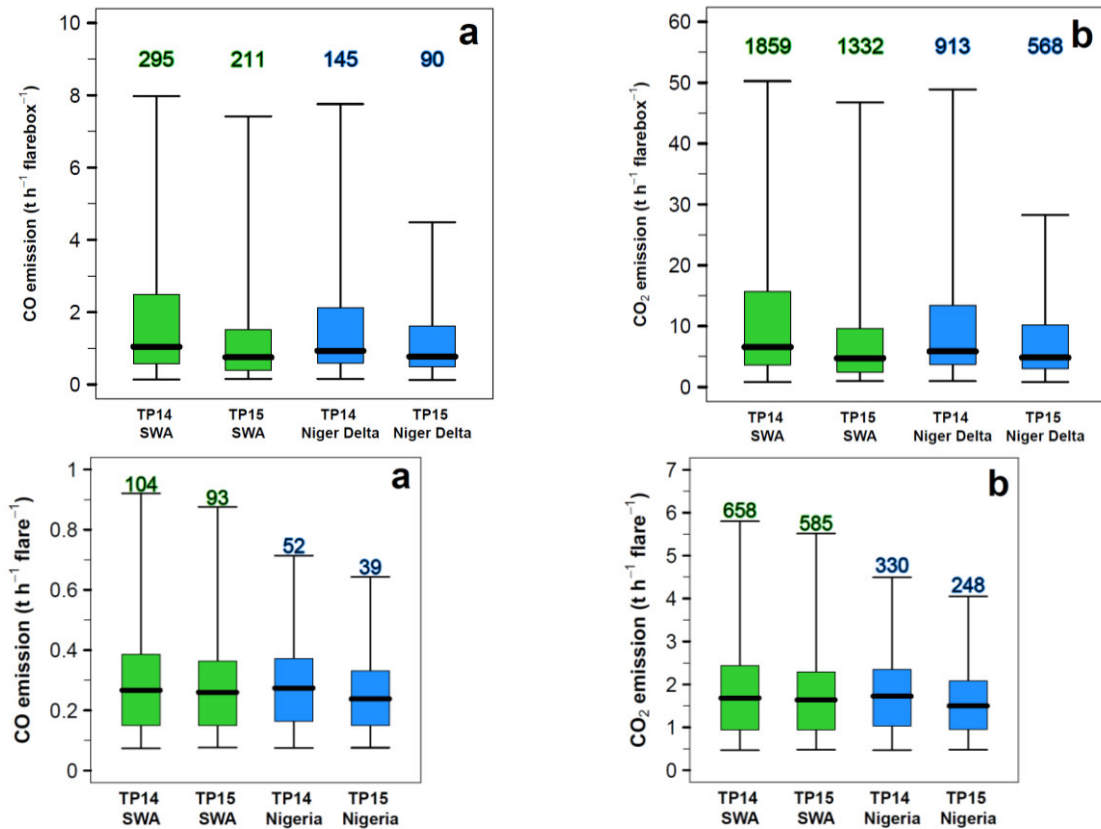
610 Fig. 8 emphasizes that the technical conditions of flaring crucially influence the emission strength and
 611 that the emissions are more sensitive towards η and δ than towards the gauge pressure.

612 3.3.3 Uncertainty due to the fraction of radiated heat

613 To estimate the uncertainty in the fraction of radiated heat f (see Tab. 2), we have used the standard
 614 deviation of the literature values given in the appendix of Guigard et al. (2000) in addition to the
 615 mean value of $f = 0.27$. This leads to a domain of uncertainty for the value f of $(^{0.38}/_{0.16})$. Therefore
 616 the $\text{VNPVNF}_{\text{flare}}$ observed radiant heat is multiplied with the factor $1/f$ of 3.7 $(^{6.2}/_{2.6})$.

620 3.3.4 Interannual variability

622 The differences in flaring between TP14 and TP15, indicated in Fig. 1 and Fig. 2, are quantified in this
 623 section according to the emissions of CO (Fig. 9a) and CO₂ (Fig. 9b). The boxplots include all flaring
 624 boxes/flares for the two domains SWA (green) and the Niger Delta area/Nigeria (blue). The numbers
 625 above indicate the integrated emissions per hour and area in tons.
 626



627 **Fig.9. Flare boxplots** Single flaring emissions of (a) CO and (b) CO₂ (E_{clim} , t h⁻¹ flare⁻¹) for SWA (green) and the Niger Delta
 628 area/Nigeria (blue) for TP14 and TP15. The values above the boxplots indicate the emissions per hour, integrated over SWA
 629 (green) and the Niger Delta area/Nigeria (blue). The whiskers span the data range from the 0.025-quantile to the 0.975-
 630 quantile (95% of the data). Data outside of this range is not shown.
 631

632
 633 The emissions of CO₂ are 6.3 times higher than the CO emissions. For SWA/Nigeria (blue boxplots) the
 634 mean value of emissions is statistically significant lower for TP15 compared to TP14 (Wilcoxon-Mann-
 635 Whitney rank sum test with a significance level of 0.05). For the Niger Delta area-SWA the emission
 636 means/averages show no significant difference. The significant different mean values for SWA
 637 emissions/Nigeria emphasize the relevance of using a flaring dataset which is up to date to reduce
 638 uncertainties arising from deviations in flare locations or flaring processes.
 639

640 3.3.5 Uncertainty due to spatial variability in H₂S

641 Since hydrogen sulfide (H₂S) is the only sulfur source in the flared gas, it determines the emission of
 642 sulfur dioxide. The natural gas composition measurements from the ten flow stations given in
 643 Sonibare and Akeredolu (2004) contain only two stations with nonzero H₂S content. Therefore
 644 averaging over the ten stations (see Tab. 3) leads to a low H₂S content in the emission calculations.
 645 By using the highest concentration value of H₂S given in Sonibare and Akeredolu (2004) (see Tab. 3,
 646 H₂S concentration 0.03% instead of 0.005%), we try to estimate the upper limit of SO₂ emission,
 647 assuming that all flares are provided with this more sulfur containing gas. With this approach the
 648

649 ~~spatiotemporal~~temporal averaged sum of SO₂ emissions over SWA increase from 0.636 to 4.9320 kg
 650 h⁻¹. ~~The maximum values in the flare boxes increase from 4.7 to 41.8 kg h⁻¹. These are rather low~~
 651 ~~values.~~

652 This comparison reveals that among the flaring conditions also the natural gas composition plays an
 653 important role in estimating the flaring emissions reasonably. To rely on a single measurement
 654 dataset for a large flaring domain and without taking into account spatial variability is therefore
 655 problematic but has to be accepted owing to ~~insufficient~~data shortage.

656 This section has estimated the uncertainties in gas flaring due to cloud cover, parameters of IU14, the
 657 fraction of radiated heat, the temporal variability and the H₂S concentration in the natural gas. The
 658 uncertainty regarding the spatial variability of the total hydrocarbon fraction of the natural gas,
 659 which is estimated by the variations in the ten flow station measurements of Sonibare and Akeredolu
 660 (2004), is below 1%.

661 However, there are further assumptions or sources of uncertainty which cannot be quantified within
 662 this study: We assume that the natural gas composition, which is measured in one region, is valid for
 663 SWA entirely. The gas flares are taken as constant emission sources because ~~VNPVNE~~VNF_{flare} only
 664 provides one observation (overflight) per day. We cannot take into account the spatial variability of
 665 the flares concerning the IU14 parameters and the stack heights. And finally IU14 delivers no VOCs
 666 and black carbon.

667

668 4. Comparison with existing emission inventories

669

670 The following section places the estimated flaring emissions of this study in the context of existing
 671 emission inventories, by taking the focus on CO₂. A direct comparison with existing emission
 672 inventories is problematic due to different reference time periods, spatial domains, definitions of
 673 emission sectors and the limitation of chemical compounds. Tab. 5 summarizes the CO₂ emissions for
 674 different inventories regarding Nigeria ~~or the Niger Delta area as denoted in Fig. 5a,~~as the flaring
 675 hotspot of the research domain. ~~The results of this study shows no flaring in the northern part of~~
 676 ~~Nigeria and therefore flaring within the Niger Delta area can be seen as the total flaring area of the~~
 677 ~~country.~~ To derive annual emission values for the results of this study, it is assumed that the flaring
 678 emission conditions of TP14 and TP15 are representative for the whole year 2014 and 2015
 679 respectively. Therefore the hourly emissions are integrated over 365 days. In addition to the three
 680 inventories E_{obsz}, E_{comz} and E_{climz}, whose emissions are derived from temporal averages of the source
 681 temperature and radiant heat, also an emission estimation using instantaneous source temperature
 682 and radiant heat (calculating emissions for every single observation and subsequent temporal
 683 averaging of the emissions) for both time periods is presented in Tab.5 (E_{climz}, instant. input).

684

685 **Tab.5.** Comparison between existing emission inventories for CO₂ (with a focus on gas flaring if available) and the results of
 686 this study for Nigeria ~~or the Niger Delta area~~ in teragram (Tg) per year. For TP14 and TP15 it is assumed that the two month
 687 observations represent the flaring conditions of the whole year 2014 and 2015 respectively. Therefore the emissions were
 688 integrated to yearly values. The ~~values in brackets represent~~domain of uncertainty arising from the upperUP14 parameters
 689 and lower limit owing to the uncertainties estimated in Section 3-spatial variability in total hydrocarbon is given in brackets.
 690 For the fraction of radiated heat f_r, the mean value 0.27 and the lower (upper) boundary of 0.16 (0.38) are used,
 691 representing a further source of uncertainty. The products given in bold are directly related to flaring emissions.

692

Emission inventory	Time period	CO ₂ emissions (Tg y ⁻¹)		
		f = 0.16	f = 0.27	f = 0.38
<u>This study (E_{obsz} averaged)</u>	<u>2014 (from TP14)</u>	<u>1.7</u> ^(2.2/0.3)	<u>1.0</u> ^(1.3/0.2)	<u>0.7</u> ^(1.0/0.1)
<u>This study (E_{comz} averaged)</u>	<u>2014 (from TP14)</u>	<u>4.5</u> ^(6.1/0.9)	<u>2.7</u> ^(3.6/0.5)	<u>1.9</u> ^(2.6/0.3)

This study (E_{clim})	2014 (from TP14)	13 ^(19/3) 4.9 (6.5/1.0)	8 ^(12/2) 2.9 (3.9/0.6)	6 ^(8/1) 2.1 (2.8/0.4)
This study (E_{obs}, averaged)	2015 (from TP15)	1.0 ^(1.4/0.2)	0.6 ^(0.8/0.1)	0.4 ^(0.6/0.0)
This study (E_{com}, averaged)	2015 (from TP15)	3.4 ^(4.5/0.7)	2.0 ^(2.7/0.4)	1.4 ^(2.0/0.3)
This study (E_{clim})	2015 (from TP15)	8 ^(12/2) 3.7 (4.9/0.7)	5 ^(7/1) 2.2 (2.9/0.4)	4 ^(5/0) 1.5 (2.1/0.3)
This study ($E_{75}E_{\text{clim}}$, instant. input)	2014 (from TP14)	7 ^(11/2) 9.9 (13.2/2.0)	45.9 (7/1) ^{7.9/1.2}	34.2 (5/0) ^{5.6/0.8}
This study ($E_{75}E_{\text{clim}}$, instant. input)	2015 (from TP15)	5 ^(7/1) 8.8 (11.8/1.8)	3 ^(4/0) 5.2 (7.0/1.0)	2 ^(3/0) 3.7 (4.9/0.7)
CDIAC (2015b)¹	2011		27.47	
EIA (2015)²	2010; 2011; 2013		38.81; 41.39; 52.83	
Doumbia et al. (2014)¹	2010		45	
EDGAR 4.2³ (ECCAD, 2015)	2008		8.75	
EDGAR 4.2⁴ (ECCAD, 2015)	2008		3.50	
EDGAR 4.3.2⁵ (EDGAR, 2016)	2010; 2011; 2012		29.4, 28.8, 28.9	
EDGARv43FT2012⁶ (EDGAR, 2014)	2014		93.87	

693
694
695
696
697
698
699
700
701
702

¹from gas flaring, Nigeria

²from consumption and flaring of natural gas

³from refineries and transformation, Nigeria

⁴from refineries and transformation, Niger Delta area according to Fig. 5a

⁵from venting and flaring of oil and gas production, Nigeria

⁶emission totals of fossil fuel use and industrial processes (cement production, carbonate use of limestone and dolomite, non-energy use of fuels and other combustion). Excluded are: short-cycle biomass burning (such as agricultural waste burning) and large-scale biomass burning (such as forest fires), Nigeria

703 The CO₂ emission estimations of this study are given in Tab. 5 together with an overall uncertainty
704 range ~~(+38/-72%) of (+33/-79%) in brackets~~, including the uncertainty from the IU14 parameters
705 η and δ ~~(+12/-52 +12/-53 %)~~ and the gauge pressure ~~(+26/-21 +20/-25 %)~~ and from spatial variability
706 of total hydrocarbon. The latter uncertainty is small (below 1%) owing to the low variation in THC
707 concentration in the measurements of Sonibare and Akeredolu (2004). ~~The uncertainty owing to the~~
708 ~~fraction of radiated heat f is represented by using the average value of 0.27 and the upper and lower~~
709 ~~estimate of 0.16 and 0.38 respectively.~~ The uncertainty due to cloud cover is represented by E_{75} .
710 ~~Regarding the relatively large uncertainty there is no preference the difference in one of the emission~~
711 ~~estimates E_{clim} and E_{obs} and E_{com} .~~
712 ~~By assuming the uncertainty range of the fraction of radiated heat f between 0.16 and 0.38, the~~
713 ~~results of the study on hand show CO₂ emissions in the same order of magnitude as~~ By assuming that
714 ~~E_{com} with $f = 0.27$ represents the best emission estimate for this study and by integrating the above~~
715 ~~mentioned sources of uncertainty, a total Nigerian CO₂ flaring emission of 2.7 (3.6/0.5) Tg y⁻¹ for 2014~~
716 ~~and 2.0 (2.7/0.4) Tg y⁻¹ for 2015 was derived. Due to the high uncertainties, the two estimates are not~~
717 ~~statistically different. These values are one order of magnitude smaller than the values from the~~
718 Carbon Dioxide Information Analysis Center (CDIAC, 2015b), the Energy Information Administration
719 (EIA, 2015) and the EDGARv.4.3.2 (EDGAR, 2016) database, ~~with best results for $f = 0.16$ but with an~~
720 ~~overall tendency to underestimate the emissions. E_{clim} shows smaller deviations to the existing~~
721 ~~inventories than the cloud correction approach of E_{75} .~~ A direct comparison is hindered by a time lag
722 of 3-4 years and missing information about the uncertainties of CDIAC. The values of EIA are higher
723 than those of CDIAC because EIA includes the consumption of natural gas in addition to gas flaring.
724 Doumbia et al. (2014) combines Defense Meteorological Satellite Program (DMSP) observations of

725 flaring with the emission factor method to derive flaring emissions. The results agree with EIA (2015)
726 but are 64% higher than CDIAC (2015b).

727 The emission inventory EDGAR v4.2 (ECCAD, 2015) delivers 8.75 (3.50) Tg CO₂ y⁻¹ for Nigeria (Niger
728 Delta area) for the emission sector *refineries and transformation*, which is in good agreement with
729 the results for the study on hand.

730 As a benchmark for the flaring CO₂, the total CO₂ emissions for Nigeria are given by EDGAR (2014),
731 (fossil fuel use and industrial processes). Taking EDGAR (2014) as a reference for total CO₂ emissions
732 of Nigeria, flaring emissions ~~contributes by 9 (13/2)% (2014; E_{clim}, f = 0.27), 14 (20/3)% (2014; E_{clim}~~
733 ~~f = 0.16) contribute with 2 (3.9/0.0)% (this study for 2014; E_{com})~~, 9% (2008; ECCAD, 2015), 28% (2011;
734 CDIAC, 2015b), 48% (2010; Doumbia et al., 2014) or 56% (2013; EIA, 2015). The large spread between
735 the different inventories emphasizes the large uncertainty within the estimation of emissions from
736 gas flaring.

737 By using the climatological approach with instantaneous source temperature and radiant heat input
738 data (E_{clim}, instant. input) instead of temporal averages (E_{clim}), the emissions are increased by approx.
739 a factor of two (5.9 (7.9/1.2) Tg y⁻¹ for 2014, 5.2 (7.0/1.0) Tg y⁻¹ for 2015). This underlines that also the
740 preprocessing of the remote sensing data for the calculation of the emissions is a considerable
741 source of uncertainty. However, due to the high uncertainties also the two emission estimates with
742 and without instantaneous data are not statistically different.

743 A shortcoming of the PEGASOS_PBL-v2 (not shown) and the EDGAR v4.2 emission inventory is the
744 lack of offshore flaring emissions in the Gulf of Guinea south of Nigeria. For CDIAC and EIA this
745 cannot be verified since the data is only available as a single value per country.

746 The differences between the results of this study and the existing emission inventories might be
747 caused by ~~an underestimation~~ insufficient information about the efficiency of the flow rate by VNP
748 and Eq. 1 combustion processes of SWA flares or by an inconsistent definition of emission source
749 sectors for the existing inventories. ~~E_{clim}, E₇₅, E_{com}~~, Doumbia et al. (2014) and CDIAC (2015b) focus on
750 gas flaring, whereas other products also include natural gas consumption and emissions from
751 refineries and transformation, which also can include non-flaring emissions within and outside the
752 areas indicated as flaring area by the satellite imagery. In addition, the existing inventories do not
753 provide current values (time lag of 2 to 6 years) and therefore not consider the emission reduction
754 indicated by Fig. 9.

755

756 5. Discussion and conclusions

757

758 The gas flaring emission estimating method of Ismail and Umukoro (2014) (IU14) has been combined
759 with the remote sensing flare location determination of the VIIRS Nightfire Prerun V2.1 Flares only
760 (~~VNPVNF~~) (VIIRS, 20152015a) for a new flaring emission parameterization. The parameterization
761 combines equations of incomplete combustion with the gas flow rate derived from remote sensing
762 parameters instead of using emission factors and delivers emissions of the chemical compounds CO,
763 CO₂, SO₂, NO and NO₂.

764 Within this study the parameterization was applied to southern West Africa (SWA) including Nigeria
765 as the second biggest flaring country. Two two-month flaring observation datasets for June-/July
766 2014 (TP14) and June/July 2015 (TP15) were used to create a flaring climatology for both time
767 periods. In this climatology all detected flares emit with their mean activity. ~~(climatological~~
768 approach).

769 The uncertainties owing to missed flare observations by cloud cover, parameterization parameters,
770 interannual variability and the natural gas compositions were assessed. It can be shown that the

771 highest uncertainties arise from the IU14 parameters (+33/-79%), followed by the definition of the
772 fraction of radiated heat f ~~and the IU14 parameters~~. The uncertainty arising from flares masked by
773 clouds is estimated as 61% on average in TP15.

774 By using ~~remote sensing the cloud cover observations~~, a correction factor for the flaring
775 climatological detection of VNF and by assuming that all cloud-covered flares are active, an
776 additional emission dataset was derived which ~~reduces~~ combines the ~~mean~~ emissions about 50%
777 from the currently observed flares and the climatological emissions from cloud-covered (not
778 detected) flares (combined approach). These emissions are on average 9% smaller than the
779 climatology but 61% larger than the net observations.

780 However, owing to the large uncertainty ranges, no significant difference between the climatological
781 inventory and the ~~cloud corrected~~ combined inventory can be stated. Comparing the emissions of
782 2014 and 2015, a reduction in the flaring area, density of active flares and a significant reduction in
783 ~~SWAN~~ Nigerian flaring emissions about 3025% can be observed, which underlines the need for more
784 recent emission inventories.

785 The uncertainty due to the natural gas composition is compound dependent. The spatial variation in
786 total hydrocarbon is negligible but the availability of hydrogen sulfide, which exclusively determines
787 the amount of emitted SO₂, cause large uncertainty. By taking the combustion efficiency to derive
788 the fraction of unburned natural gas, the amount of emitted VOCs might be estimated in addition to
789 the species of the study on hand but would also be linked to high uncertainties concerning the VOC
790 speciation. The uncertainty in VOC emission is increased drastically by natural gas which is vented
791 directly into the atmosphere instead of being flared, since the venting cannot be detected by
792 ~~VNP~~ VNF.

793 With a focus on Nigeria, the CO₂ emission estimates of this study were compared with existing
794 inventories. For the ~~climatology~~ combined approach, CO₂ emissions of ~~8 (12/2) 2.7 (3.6/0.5)~~ Tg y⁻¹ for
795 2014 and ~~5 (7/1) 2.0 (2.7/0.4)~~ Tg y⁻¹ for 2015 were derived. EDGAR v4.2 for the year 2008 shows the
796 same order of magnitude when limiting to emissions from refineries and transformation. The results
797 of this study are one order of magnitude smaller compared to CDIAC (Carbon Dioxide Information
798 Analysis Center) ~~is in the same order of magnitude as the results of this study~~. Doumbia et al. (2014)
799 and EIA (Energy Information Administration) ~~show emissions which are 2.4 and 2.8 times higher than~~
800 ~~the results~~. This emission underestimation is not caused by an underestimation of the flared gas
801 volume. VNF_{flare} includes an estimation of the annual sum of flared gas by country. For Nigeria the
802 estimated values are 8.56 (7.64) bcm flared gas in 2014 (2015). Within this study ~~higher values of~~
803 ~~37.89 (20.68) bcm for 2014 (2015) are derived~~.

804 The deviations might be caused by ~~uncertainties~~ the uncertainty in the ~~flow rate~~ derived by VNP
805 ~~radiant heat, which can be assessed only rudimentary via the parameter~~ efficiency of the fraction of
806 ~~radiated heat~~ flares concerning the combustion process and their operation. A lack of information
807 regarding the combustion efficiency together with the high sensitivity of the parameters within the
808 combustion equations of IU14 can lead to high uncertainties. Additionally, the usage of emission
809 factors in the existing inventories which did not take into account the spatiotemporal variability of
810 flaring, inconsistent emission sector definitions or the time lag of the emission inventories of 2-5
811 years can ~~lead to~~ cause deviations. The positive trend in Nigerian gas flaring CO₂ emissions derived by
812 EIA from 38.81 to 52.83 Tg y⁻¹ between 2010 and 2013 contradicts the findings of Doumbia et al.
813 (2014) and this study, which generally show a decrease in emissions from 1994 to 2010 and from
814 2014 to 2015, respectively. Based on the sensitivity study, which reveals high uncertainties of the
815 flaring emission, we conclude that there is no preference in the choice of ~~one of the~~ emission

816 | [estimates climatological and or the combined approach](#) presented in this study. Therefore [for](#)
817 | [simplicity](#) we recommend the use of the climatological approach when using the R package.

818 | Despite the generally large uncertainties in the estimation of emissions from gas flaring, this method
819 | allows a flexible creation of flaring emission datasets for various applications (e.g. as emission
820 | inventory for atmospheric models). It combines observations with physical based background
821 | concerning the combustion. The use of current data makes it possible to consider present trends in
822 | gas flaring. Even the creation of near real-time datasets with a time lag of one day is possible. The
823 | emissions are merged on grid predefined by the user and depending on the availability of [VNP/VNF](#)
824 | data, the temporal resolution can be selected from single days to years.

825 | An improvement of this parameterization can be achieved by an extension of the IU14 method to
826 | black carbon and VOCs and an inclusion of spatial resolved measurements of the natural gas
827 | composition in combination with information of the gas flaring processes from the oil producing
828 | industry.

829

830 | **Acknowledgments**

831

832 | The research leading to these results has received funding from the European Union 7th Framework
833 | Programme (FP7/2007-2013) under Grant Agreement no. 603502 (EU project DACCIWA: Dynamics-
834 | aerosol-chemistry-cloud interactions in West Africa).

835 | [We thank Mikhail Zhizhin from Earth Observation Group \(EOG\) of NOAA for providing us with the](#)
836 | [extracted flaring information from the VNF product.](#) We are grateful to Godsgift Ezaina Umukoro
837 | (Department of Mechanical Engineering, University of Ibadan, Nigeria) for the kind support during
838 | the implementation of their combustion reaction theory into our parameterization. ~~[We also thank](#)~~
839 | ~~[the Earth Observation Group \(EOG\) of NOAA for providing the VIIRS Nightfire Flares Only product.](#)~~

840

841 | **Code and/or data availability**

842 |

843 | This publication includes a package of well documented R scripts which is free available for research
844 | purposes and enables the reader to create their own gas flaring emission datasets. It includes
845 | exemplarily the preprocessing for June-/July 2015 with a focus on southern West Africa. You get
846 | access to the code via zenodo.org (DOI: 10.5281/zenodo.~~50938~~-61151), [entitled "Gas flaring](#)
847 | [emission estimation parameterization v2"](#).

848

849 | **References**

850

851 | API, 2007: **Pressure-relieving and Depressuring Systems**, ANSI/API STANDARD 521 FIFTH EDITION,
852 | JANUARY 2007, ISO 23251 (Identical), Petroleum and natural gas industries – Pressure-relieving and
853 | depressuring systems, American Petroleum Institute, Section 7.3.2.4: Design details h), 127
854

855 | Bader, A., Baukal, C. E., Bussman, W. Zink, J., 2011: **Selecting the proper flare systems**, American
856 | Institute of Chemical Engineers (AIChE), <http://people.clarkson.edu/wwilcox/Design/FlareSel.pdf>,
857 | accessed: October 2, 2014
858

859 | CDIAC, 2015a: **Global CO2 Emissions from Fossil-Fuel Burning, Cement Manufacture, and gas**
860 | **Flaring: 1751-2008**, Carbon Dioxide Information Analysis Center (CDIAC),
861 | http://cdiac.ornl.gov/ftp/ndp030/global.1751_2008.ems, accessed: December 6, 2015
862

863 CDIAC, 2015b: **National CO₂ Emissions from Fossil-Fuel Burning, Cement Manufacture, and gas**
864 **Flaring: 1751-2011**, Carbon Dioxide Information Analysis Center (CDIAC), Fossil-Fuel CO₂ Emissions by
865 Nation, http://cdiac.ornl.gov/ftp/ndp030/nation.1751_2011.ems, accessed: December 3, 2015
866

867 CM SAF, 2015: **Operational Products: CFC – Fractional cloud cover instantaneous data** (MSG disk,
868 CM SAF definition), Version 350;
869 [https://wui.cmsaf.eu/safira/action/viewPeriodEntry?id=11495_14063_15657_15672_16574_19152_](https://wui.cmsaf.eu/safira/action/viewPeriodEntry?id=11495_14063_15657_15672_16574_19152_20532_21207)
870 [20532_21207](https://wui.cmsaf.eu/safira/action/viewPeriodEntry?id=11495_14063_15657_15672_16574_19152_20532_21207), accessed: November 25, 2015
871

872 Doumbia, T., Granier, L., Liousse, C., Granier, C., Rosset, R., Oda, T., Fen Chi, H., 2014: **Analysis of fifty**
873 **year Gas flaring Emissions from oil/gas companies in Africa**, AGU Fall Meeting 2014, Dec 2014, San
874 Francisco, United States. A13E-3217
875

876 Dung, E. J., Bombom, L. S., Agusomu, T. D., 2008: **The effects of gas flaring on crops in the Niger**
877 **Delta, Nigeria**, *GeoJournal*, Vol., 73, 297-305
878

879 Ekpoh, I. J., Obia, A. E., 2010: **The role of gas flaring in the rapid corrosion of zinc roofs in the Niger**
880 **Delta Region of Nigeria**, *Environmentalist*, Vol. 30, 347-352
881

882 ECCAD, 2015: **Emissions of atmospheric compounds & compilation of ancillary data (ECCAD)**,
883 http://eccad.sedoo.fr/eccad_extract_interface/JSF/page_critere.jsf, accessed: December 4, 2015
884
885

886 EDGAR, 2016: **Global Emissions EDGAR v4.3.2**, European Commission, Joint Research Centre
887 (JRC)/PBL Netherlands Environmental Assessment Agency. Emission Database for Global Atmospheric
888 Research (EDGAR), release version 4.3.2. <http://edgar.jrc.ec.europa.eu>
889

890 EDGAR, 2014: **Global Emissions EDGAR v4.3 FT2012**, European Commission, Joint Research Centre
891 (JRC)/PBL Netherlands Environmental Assessment Agency. Emission Database for Global Atmospheric
892 Research (EDGAR), release version 4.3. <http://edgar.jrc.ec.europa.eu>, 2015 forthcoming,
893 <http://edgar.jrc.ec.europa.eu/overview.php?v=CO2ts1990-2014>, accessed: December 3, 2015
894

895 EIA, 2015: **CO₂ from the Consumption and Flaring of Natural Gas**, International Energy Statistics,
896 U.S. Energy Information Administration (EIA),
897 [http://www.eia.gov/cfapps/ipdbproject/iedindex3.cfm?tid=90&pid=3&aid=8&cid=&syid=2010&eyid](http://www.eia.gov/cfapps/ipdbproject/iedindex3.cfm?tid=90&pid=3&aid=8&cid=&syid=2010&eyid=2013&unit=MMTCD)
898 [=2013&unit=MMTCD](http://www.eia.gov/cfapps/ipdbproject/iedindex3.cfm?tid=90&pid=3&aid=8&cid=&syid=2010&eyid=2013&unit=MMTCD), accessed: December 3, 2015
899

900 Elvidge, C. D., Zhizhin, M., Baugh, K., Hsu, F.-C., Gosh, T., 2015: **Methods for Global Survey of Natural**
901 **Gas Flaring from Visible Infrared Imaging Radiometer Suite Data**, *Energies* 2016, 9, 14, 1-15
902

903 Elvidge, C. D., Zhizhin, M., Hsu, F.-C., Baugh, K. E., 2013: **VIIRS Nightfire: Satellite Pyrometry at Night**,
904 *Remote Sens.*, Vol. 5, 4423-4449
905

906 Elvidge, C. D., Ziskin, D., Baugh, K. E., Tuttle, B. T., Gosh, T., Pack, D. W., Erwin, E. H., Zhizhin, M.,
907 2009: **A fifteen year record of global natural gas flaring derived from satellite data**, *Energies*, Vol. 2,
908 595-622
909

910 Elvidge, C. D., Baugh K. E., Kihn, E. A., Kroehl, H. W., Davis, E. R., 1997: **Mapping city lights with**
911 **nighttime data from the DMSP operation linescan system**, *Photogrammetric Engineering & Remote*
912 *Sensing*, Vol. 63, No. 6, 727-744
913

914 EPA, 1985: **Evaluation of the efficiency of industrial flares: Flare head design and gas composition**,
915 Research and Development, United States Environmental Protection Agency (EPA), EPA-600/2-85-
916 106, Tab. 2-6
917

918 Google Earth, 2014: Image 2014 DigitalGlobe, <http://www.earth.google.com>
919

920 Guigard, S. E., Kindzierski, W. B., Harper, N., 2000: **Heat Radiation from Flares**. Report prepared for
921 Science and Technology Branch, Alberta Environment, ISBN 0-7785-1188-X, Edmonton, Alberta.
922

923 Ismail, O. S., Umukoro, G. E., 2014: **Modelling combustion reactions for gas flaring and its resulting**
924 **emissions**, Journal of King Saud University – Engineering Sciences, Vol. 28, 130-140
925

926 Johnson, M. R., Devillers, R. W., Thomson, K. A., 2011: **Quantitative Field Measurements of Soot**
927 **Emission from Large Gas Flare using Sky-LOSA**, Environ. Sci. Technol., Vol. 45, 345-350
928

929 Knippertz, P., Evans, M. J., Field, P. R., Fink, A. H., Liousse, C., Marsham, J. H., 2015: **The possible role**
930 **of local air pollution in climate change in West Africa**, Nature Climate Change, Vol. 5, 815-822
931

932 Mirador, 2016: AIRS/Aqua Level 2 Standard physical retrieval (AIRS+AMSU), Total cloud fraction
933 (CldFrcTot), [mirador.gsfc.nasa.gov/cgi/bin/mirador/presentNavigation.pl?tree=project&](http://mirador.gsfc.nasa.gov/cgi/bin/mirador/presentNavigation.pl?tree=project&Project=AIRS&data)
934 [Project=AIRS&data](http://mirador.gsfc.nasa.gov/cgi/bin/mirador/presentNavigation.pl?tree=project&Project=AIRS&data), accessed: April 18, 2016
935

936 NASA, 2016: <http://npp.gsfc.nasa.gov/viirs.html>, accessed: January 5, 2016
937

938 Nwankwo, C. N., Ogagarue, D., O., 2011: **Effects of gas flaring on surface and ground waters in Delta**
939 **State Nigeria**, Journal of Geology and Mining Research, Vol. 3, 131-136
940

941 Nwaugo, V. O., Onyeagba, R. A., Nwahcukwu, N. C., 2006: **Effect of gas flaring on soil microbial**
942 **spectrum in parts of Niger Delta area of southern Nigeria**, African Journal of Biotechnology, Vol. 5,
943 1824-1826
944

945 Osuji, L. C., Avwiri, G. O., 2005: **Flared Gas and Other Pollutants Associated with Air quality in**
946 **industrial Areas of Nigeria: An Overview**, Chemistry & Biodiversity, Vol. 2, 1277-1289
947

948 R Core Team, 2013: **R: A Language and Environment for Statistical Computing**, R Foundation for
949 Statistical Computing, Vienna, Austria, <http://www.R-project.org/>
950

951 Sonibare, J. A., Akeredolu, F. A., 2004: **A theoretical prediction of non-methane gaseous emissions**
952 **from natural gas combustion**, Energy Policy, Vol. 32, 1653-1665
953

954 Strosher, M. T., 2000: **Characterization of Emissions from Diffuse Flare Systems**, Journal of the Air &
955 Waste Management Association, 50:10, 1723-1733
956

957 Strosher, M. T., 1996; **Investigations of flare gas emissions in Alberta**, Final Report to: Environment
958 Canada, Conservation and protection, the Alberta Energy and Utilities Board, and the Canadian
959 Association of Petroleum Producers; Environmental Technologies, Alberta Research Council, Calgary,
960 Alberta
961

962 ~~TA-Luft, 1986: **Technische Anleitung zur Reinhaltung der Luft 1986**. Heider-Verlag, 5060 Bergisch
963 Gladbach 2, Anhang C: Ausbreitungsrechnung, Eq. 2.1, 127-139~~
964

965 van der Linden, R., Fink, A. H., Redl, R., 2015: **Satellite-based climatology of low-level continental**
966 **clouds in southern West Africa during the summer monsoon season**, Journal of Geophysical
967 Research: Atmospheres, Vol. 120, 1186-1201
968

969 [VDI 3782, 1985: Dispersion of Air Pollutants in the Atmosphere, Determination of Plume rise, Verein](#)
970 [Deutscher Ingenieure, VDI-Richtlinien 3782 Part 3, Equation 24, https://www.vdi.de/richtlinie/](#)
971 [vdi 3782 blatt 3-ausbreitung von luftverunreinigungen in der atmosphaere berechnung der](#)
972 [abgasfahnenueberhoehung/](#), accessed: October 17, 2016
973
974 VIIRS, ~~2015~~2015a: http://ngdc.noaa.gov/eog/viirs/download_viirs_fire.html, accessed: August 24,
975 [2016](#)
976
977 [VIIRS, 2015b: http://ngdc.noaa.gov/eog/viirs/download_viirs_flares_only.html](#), accessed: ~~November~~
978 [July 31](#), 2015
979
980 Vogel, B., Vogel, H., Bäumer, D., Bangert, M., Lundgren, K., Rinke, R., Stanelle, T., 2009: **The**
981 **comprehensive model system COSMO-ART - Radiative impact of aerosol on the state of the**
982 **atmosphere on the regional scale**, Atmos. Chem. Phys., 9, 8661-8680
983
984 World Bank, 2012: [http://www.worldbank.org/content/dam/Worldbank/Programs/Top 20 gas](http://www.worldbank.org/content/dam/Worldbank/Programs/Top_20_gas)
985 [flaring countries.pdf](#), accessed: December 5, 2015
986
987 Zhang, X., Scheving, B., Shoghli, B., Zygarlicke, C., Wocken, C., 2015: **Quantifying Gas Flaring CH₄**
988 **Consumption Using VIIRS**, Remote Sens., Vol. 7, 9529-9541
989